CELL BIOLOGY

A cell-based GEF assay reveals new substrates for DENN domains and a role for DENND2B in primary ciliogenesis

Rahul Kumar*, Vincent Francis, Gopinath Kulasekaran, Maleeha Khan, Gary A. B. Armstrong, Peter S. McPherson*

Primary cilia are sensory antennae crucial for cell and organism development, and defects in their biogenesis cause ciliopathies. Ciliogenesis involves membrane trafficking mediated by small guanosine triphosphatases (GTPases) including Rabs, molecular switches activated by guanine nucleotide exchange factors (GEFs). The largest family of Rab GEFs is the DENN domain–bearing proteins. Here, we screen all 60 Rabs against two major DENN domain families using a cellular GEF assay, uncovering 19 novel DENN/Rab pairs. The screen reveals Rab10 as a substrate for DENND2B, a protein previously implicated in cancer and severe mental retardation. Through activation of Rab10, DENND2B represses the formation of primary cilia. Through a second pathway, DENND2B functions as a GEF for RhoA to control the length of primary cilia. This work thus identifies an unexpected diversity in DENN domain–mediated activation of Rabs, a previously unidentified non-Rab substrate for a DENN domain, and a new regulatory protein in primary ciliogenesis.

INTRODUCTION

Vesicle trafficking is a fundamental cellular process involving the transport of lipids and proteins throughout cells using a series of trafficking events including vesicle budding from donor organelles, vesicle transport, and fusion of vesicles with acceptor compartments. The spatial and temporal control of these events is largely mediated by the Rab family of small guanosine triphosphatases (GTPases), which regulate all aspects of membrane trafficking at all cellular locations (*1*).

Mammalian cells have approximately 60 Rabs (*2*). Rabs switch between a guanosine triphosphate (GTP)–bound active state and a guanosine diphosphate (GDP)–bound inactive state (*3*). These switches are controlled by guanine nucleotide exchange factors (GEFs) and GTPase-activating proteins (GAPs). Upon activation by GEFs, Rabs carry out their appropriate membrane trafficking functions, recruiting effector proteins that drive trafficking events (*3*). The association of Rab GTPases with membranes requires insertion of hydrophobic geranylgeranyl groups, attached to one or two cysteine residues at the C terminus of Rabs into the cytosolic leaflet (*4*). Upon inactivation by GAPs, which stimulate the intrinsic GTPase activity, Rabs are extracted from the membrane and interact reversibly with the molecular chaperone GDP dissociation inhibitor (GDI) to form a cytosolic complex, protecting the hydrophobic moieties (*5*, *6*).

Because the presence of a specific Rab on an organelle is a defining feature of that organelle, a key question relates to how Rabs are targeted to their appropriate cellular location. Early studies suggested a role of the hypervariable region at the C terminus of the Rab as a targeting signal (*7*). However, this was challenged as the hypervariable region can be dispensable for Rab membrane targeting (*8*). It has also been postulated that GDI displacement factors (GDFs) drive dissociation of Rab-GDP/GDI complexes, catalyzing Rab membrane delivery (*9*). However, only one GDF has been identified

(*10*). It is thus unclear how this process could mediate the distinct membrane targeting of multiple Rabs. It was subsequently demonstrated that the GEF DrrA recruits Rab1 to membranes by catalyzing GTP loading, leading to displacement of GDI, without the need of a GDF (*11*). Moreover, when GEFs are artificially relocated to membranes of different organelles, such as mitochondria, substrate Rabs are mistargeted to these new locations (*12*). GEF-mediated activation of Rabs drives Rab membrane association and allows the GTPases to recruit and trap effector proteins (*13*). These experiments suggest that GEFs are solely responsible for controlling the spatial and temporal localization of Rab GTPases and thus their effectors.

There are far fewer GEFs than Rabs (*14*). The largest family of GEFs are those bearing a DENN (differentially expressed in normal and neoplastic cells) domain, an evolutionary conserved protein module (*15*). There are minimally 18 members in the DENN domain family that are further divided into eight subfamilies, most of which are poorly characterized (*15*). A screen of 16 DENN domain proteins against most Rabs using an in vitro approach led to the assignment of a single, unique Rab to each DENN domain subfamily (*16*). However, subsequent cell biological studies focused on individual DENN domain proteins including DENND1C (*17*, *18*) and DENND2B (*19*) revealed different Rab substrates than those identified in the in vitro screen. In vitro GEF assays are challenging in that purification of recombinant Rabs can lead to inactivation and altered nucleotide loading (*20*), and purified DENN domains may also be misfolded.

Here, we develop a cell-based GEF assay to identify Rab GTPase substrates of the seven members of the DENND1 and DENND2 families, using a mitochondrial relocalization approach. Screening against 60 Rabs reveals that each member of the DENND1/DENND2 families activates multiple GTPases, changing the notion that each DENND family targets one common Rab (*16*, *18*).

Multiple Rab GTPases are associated with trafficking of proteins regulating the formation of primary cilia (*21*). Primary cilia are microtubule-based nonmotile sensory organelles present in most vertebrates. These organelles are critical in regulating signal transduction pathways including Hedgehog (Hh) signaling (*22*). Disruption in ciliogenesis leads to a spectrum of disorders known as ciliopathies,

Department of Neurology and Neurosurgery, Montreal Neurological Institute (the Neuro), McGill University, Montreal, Quebec, Canada.
*Corresponding author. Email: peter.mcpherson@mcgill.ca (P.S.M.); rahul.kumar@mail.mcgill.ca (R.K.)

including polycystic kidney disease, skeletal malformations, retinal degeneration, mental retardation, and cancer (*23*). Cells form primary cilia by two pathways: (i) the extracellular pathway where the basal body (matured mother centriole) docks to the apical plasma membrane and cilia form from the apical plasma membrane and (ii) the intracellular pathway in which the basal body fuses with ciliary vesicles, allowing cilia formation in the cytoplasm, which eventually fuse with the apical plasma membrane (*24*). The maturation of the mother centriole requires encapsulation by ciliary vesicles from the Golgi (*25*), implicating Rab-mediated trafficking. Several Rab GTPases and their GEFs have been described as positive regulators of ciliogenesis (*26*). In addition, there is a critical negative regulatory pathway in ciliogenesis. Specifically, the centriolar coiled-coil protein of 110 kDa (CP110), along with associated proteins, caps the basal body and prevents cilia growth. How this pathway is regulated is unknown.

Here, we found that DENND2B (also known as suppression of tumorigenicity 5), via activation of Rab10, inhibits primary cilia formation through Rab10-dependent recruitment of the inhibitor CP110 to the mother centriole. Through a second pathway, involving direct enzymatic activation of RhoA, DENND2B controls ciliary length. The importance of DENND2B is illustrated with the finding that patients with a loss-of-function mutation in DENND2B display mental retardation and multiple congenital abnormalities (*27*). Thus, we have found unexpected diversity in DENN domain control of small GTPases leading to a new regulatory mechanism for primary ciliogenesis.

RESULTS

Identification of Rab substrates of the DENND1 and DENND2 families

To identify DENN substrates, we screened all members of the DENND1 and DENND2 subfamilies against all 60 Rab GTPases using a mitochondrial recruitment assay. Given that the isolated DENN domain is solely responsible for GEF activity (*18*), the assay involves targeting DENN domains to the mitochondrial outer surface by fusion with amino acids 141 to 187 of ActA from *Listeria monocytogenes* (Fig. 1A) (*28*). We verified that the mito-chondrial targeted DENN domain of DENND1A [DENN(1A)-mito] is recruited selectively to mitochondria (fig. S1), where it leads to a near-complete steady-state relocalization of cotransfected GFP-Rab35 (Fig. 1, B and C). A nonprenylatable form of Rab35 lacking the two C-terminal cysteines (GFP-Rab35 C_C del) is not recruited to the mitochondria (Fig. 1D), indicating that mitochondrial recruitment of the GTPase requires membrane insertion of prenyl groups. This indicates that Rab35 is inserted into the mitochondrial membrane via a GEF activity and is not simply trapped via DENN domain binding. To visualize Rab35 recruitment in real time, we developed an inducible system based on heterodimerization of the FK506-binding protein domain (FKBP) from the human FKBP12 protein and the FKBP-rapamycin–binding domain (FRB) of mTOR (mammalian target of rapamycin) (fig. S2A). Upon addition of rapamycin, each of DENND1A, DENND1B, and DENND1C rapidly translocates to mitochondria where they recruit Rab35, indicating that all three DENND1 DENN domains function as Rab35 GEFs (Fig. 1E; fig. S2, B to D; and movie S1).

We next cotransfected HeLa cells with individual DENN-mito and GFP-Rab constructs (Fig. 2A and fig. S3) in a 7 by 60 screen and
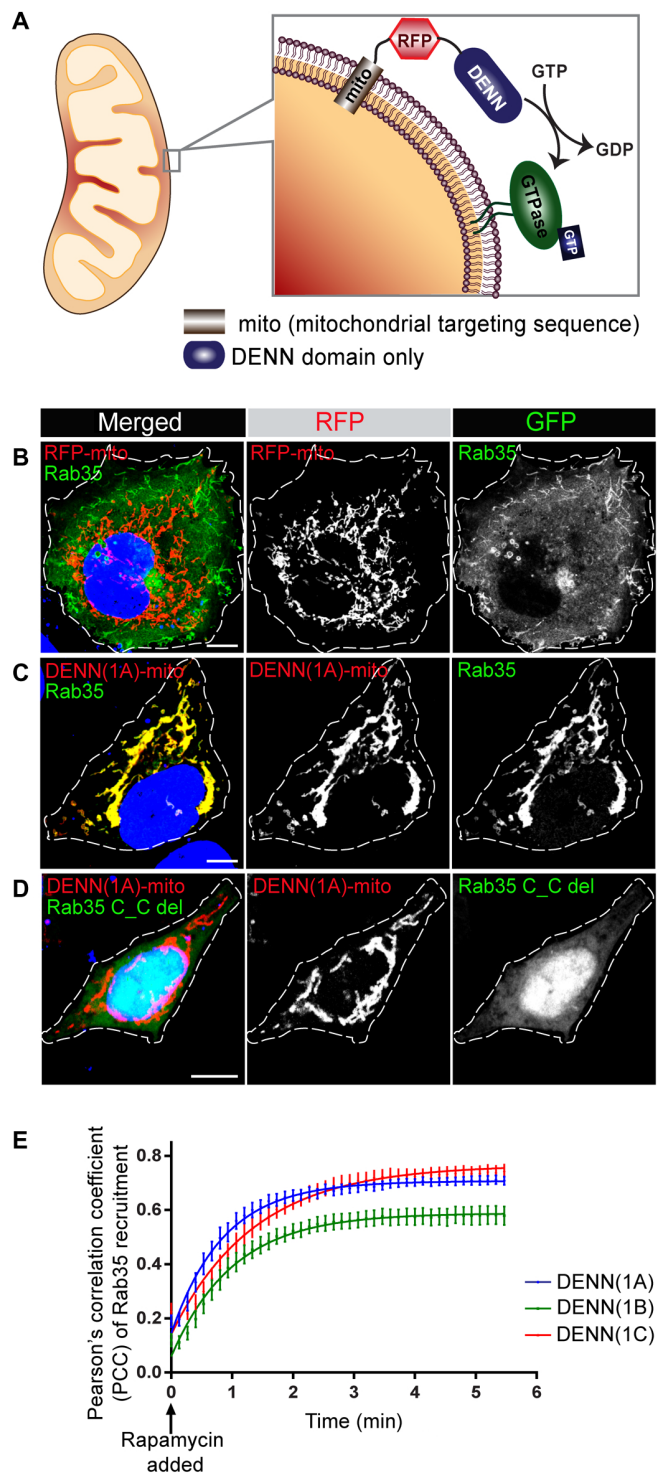

Fig. 1. DENN domains targeted to mitochondria recruit their Rab substrates. (**A**) Schematic model of the cell-based GEF assay. (**B** and **C**) HeLa cells cotransfected with GFP-Rab35 and RFP-mito (B) or GFP-Rab35 and DENN(1A)-mito (C) were stained with 4′,6-diamidino-2-phenylindole (DAPI) to reveal nuclei. (**D**) HeLa cells cotransfected with DENN(1A)-mito and GFP-Rab35 C_C del were stained with DAPI (blue) to reveal nuclei. Scale bars, 8 μm. (**E**) Curves demonstrating the recruitment kinetics of Rab35 (means ± SEM from 12 independent experiments). Recruitment curves were fit by a nonlinear regression one-phase association.
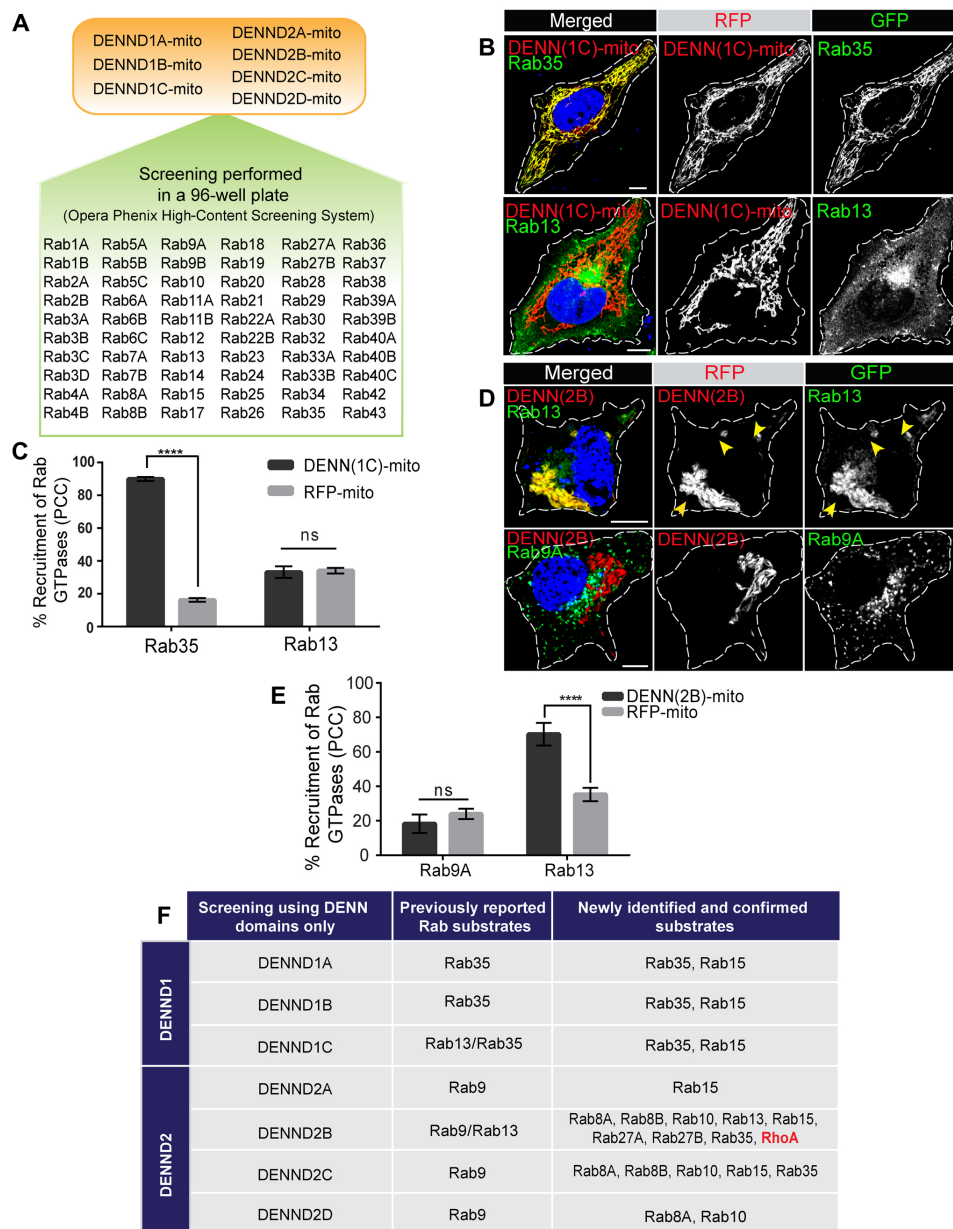
Fig. 2. High-content screening reveals GEF activity of DENND1 and DENND2 DENN domains. (**A**) Schematic representation of a comprehensive screen of DENN(1A/1B/1C) and DENN(2A/2B/2C/2D) against 60 GFP-Rabs. (**B**) HeLa cells coexpressing DENN(1C)-mito and GFP-Rab35 or GFP-Rab13 were stained with DAPI to reveal nuclei. Scale bars, 8 μm. (**C**) Quantification of percentage recruitment of Rab35 and Rab13 by DENN(1C) by analyzing colocalization using PCC (Pearson correlation coefficient) measuring cells from six independent experiments as shown in (B); means ± SEM; unpaired *t* test (for Rab35) and Welch *t* test (for Rab13); ****$P < 0.001$; ns, not significant. (**D**) HeLa cells expressing DENN(2B)-mito and GFP-Rab13 or GFP-Rab9A were stained with DAPI to reveal nuclei. Scale bars, 8 μm. (**E**) Quantification of percentage recruitment of Rab9A and Rab13 by DENN(2B) by analyzing colocalization using PCC, measuring cells from five independent experiments as shown in (D); means ± SEM; unpaired *t* test (for Rab13) and Mann-Whitney *U* test (for Rab9A); ****$P < 0.001$. (**F**) Tabular representation of all the newly identified or confirmed GTPases recruited by the respective DENN domain proteins versus previously reported GTPases.

compared the mitochondrial localization of the GFP-Rabs in the presence of the DENN domain red fluorescent protein (RFP)–mito (Fig. 2, A to F) or a control RFP-mito (fig. S4). All three members of the DENND1 family (1A/1B/1C) recruit Rab35 to the mitochondria (Fig. 2B and fig. S5, A and B). Unexpectedly, the screen also revealed Rab15 as a substrate for all three DENND1 DENN domains (figs. S5, C to E, and S6). Note that Rab35 and Rab15 have largely overlapping subcellular localizations (early and recycling endosomes)

and function (endocytic recycling) (*18*, *29*, *30*). Apart from Rab35 and Rab15, the three DENND1 DENN domains recuit no other Rabs (fig. S6). Notably, DENN(1C) does not recruit Rab13 (Fig. 2, B and C) (*16*).

Screening of the four members of the DENND2 subfamily against all 60 Rabs (Fig. 2A) revealed an array of Rab substrates. DENND2A selectively recruited Rab15 (figs. S7A and S8). DENND2B recruited Rab8A, Rab8B, Rab10, Rab13, Rab15, Rab27A, Rab27B, and Rab35 (Fig. 2D and figs. S7, B to F, and S8). DENND2C recruited

Rab8A, Rab8B, Rab10, Rab15, and Rab35 (figs. S7, G to J, and S8). Last, DENND2D recruited Rab8A and Rab10 (figs. S7, K and L, and S8). There is commonality among these substrates as they all function in delivery of cargo to the plasma membrane, either through recycling pathways or directly via the secretory pathway (18, 19, 31). However, there is no obviously phylogenetic or structural relationship such that substrate specificity remains unclear. Among the targets for DENN(2B) was Rab13 (Fig. 2D) (19). In contrast, we did not detect recruitment of Rab9 to mitochondria by DENN(2B) (Fig. 2, D and E) (16) or other members of the DENND2 family (Fig. 2F and fig. S8).

Loss of DENND2B promotes primary cilia formation and enhanced cilia length

A loss-of-function mutation in DENND2B is seen in a patient with submucous cleft palate, unilateral cystic kidney dysplasia, sensorineural hearing loss, persistent ductus Botalli, mental retardation, and other anomalies (27), symptoms associated with a ciliopathy. Ciliopathies are a group of disorders caused by the dysfunction of primary cilia (23, 32). In addition, DENND2B has a role in cancer invasion (19), a phenotype associated with primary cilia defects (33). Rab8, Rab10, and Rab35 each regulate distinct aspects of primary ciliogenesis (26, 34–36), and all were recruited to mitochondria with the DENND2B DENN domain. Thus, we sought to explore whether DENND2B regulates the formation or function of primary cilia.

The formation of primary cilia is induced in cultured cells by serum starvation (37). We transfected human alveolar epithelial cells (A549), a model for primary cilia formation (38) with GFP-DENND2B; induced ciliogenesis by serum starvation; and labeled cells with markers of the centrosome and primary cilia. The centrosome is the major microtubule-organizing center in animal cells and is composed of two centrioles, the mother and daughter centrioles, MC and DC, respectively. Each centriole has a proximal and a distal end. Upon serum starvation, the distal end of the mother centriole matures into a basal body and initiates primary cilia formation (39). While most DENND2B localizes to the cell periphery (19), a pool of approximately 2% colocalizes with gamma-tubulin (γ-tubulin), a marker of the proximal end of the basal body (Fig. 3, A and B). This DENND2B pool is proximal to CEP164, a marker of the distal appendage (a structural protrusion at the distal end of the basal body involved in membrane docking) of the mother centriole (Fig. 3, C and D) (40). DENND2B does not localize to the cilium proper as marked by acetylated tubulin (Ac-tubulin) (Fig. 3E). As revealed by staining for Ac-tubulin, cells overexpressing DENND2B have a reduced percentage of primary cilia compared to GFP transfected cells (fig. S9, A and B). Moreover, the length of the cilia is reduced (fig. S9C). In addition, note that most cells having DENND2B localized at the ciliary base lack primary cilia (fig. S9A). These data suggest that DENND2B functions as a repressor of primary cilia formation.

We used CRISPR-Cas9 to knockout (KO) DENND2B in A549 cells, which we validated with genomic sequencing and immunoblot (fig. S10, A to C). A549 KO cells had a higher percentage of ciliated cells and longer primary cilia as compared to wild-type (WT) cells (Fig. 4, A to C). Similar results were seen in DENND2B KO human retinal pigment epithelial-1 (RPE-1) cells (fig. S10, D to F, and Fig. 4, D to F). Expression of GFP-DENND2B in the DENND2B KO cells rescues both the percentage of ciliated cells and ciliary length, thus ruling
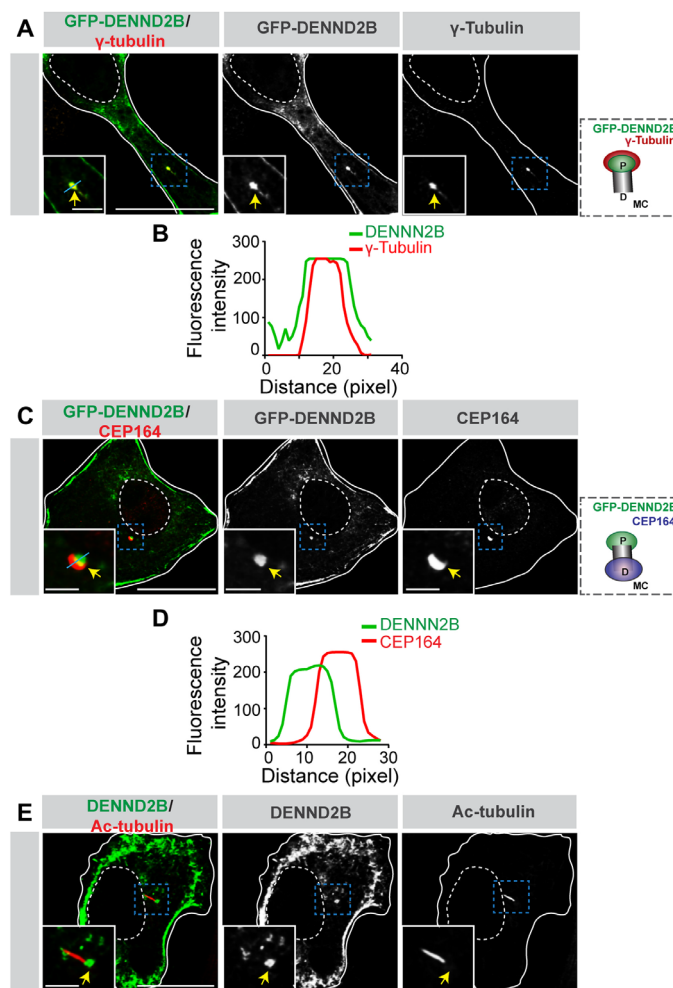

Fig. 3. DENND2B localizes at the proximal end of the mother centriole. (**A**) A549 cells with GFP-DENND2B were starved and then stained with γ-tubulin antibody to mark the basal body. The nucleus and cell periphery are outlined. Scale bars, 20 and 3 μm for low- and high-magnification images, respectively. (**B**) Intensity profiles along the straight blue line from the inset image in (A). (**C**) A549 cells with GFP-DENND2B were starved and then stained with CEP164 antibody to reveal the distal end of the mother centriole. The nucleus and cell periphery are outlined. Scale bars, 20 and 2.7 μm for low- and high-magnification images, respectively. The yellow arrows show localization of DENND2B proximal to the CEP164 staining. (**D**) Intensity profiles along the straight blue line from the inset image in (C). (**E**) A549 cells with GFP-DENND2B were starved and then stained with Ac-tubulin antibody to reveal primary cilia. The nucleus and cell periphery are outlined. Scale bars, 20 and 3.5 μm for low- and high-magnification images, respectively. The yellow arrows show localization of DENND2B at the base of primary cilia staining. For schematic representations of the mother centriole, "P," proximal end of the centriole; "D," distal end of the centriole; and "MC," mother centriole.

out the possibility of off-target effects (fig. S11, A to C). Collectively, the overexpression and KO/rescue studies indicate that DENND2B plays an inhibitory role in primary cilia formation and length.

We next examined whether the function of DENND2B in primary ciliogenesis is evolutionarily conserved and observable in an in vivo model. Alignment of full-length DENND2B from zebrafish and human revealed ~65% sequence identity with ~90% identity in the DENN domain. We injected either an antisense morpholino (MO) oligonucleotide blocking translation of the *dennd2b* transcript
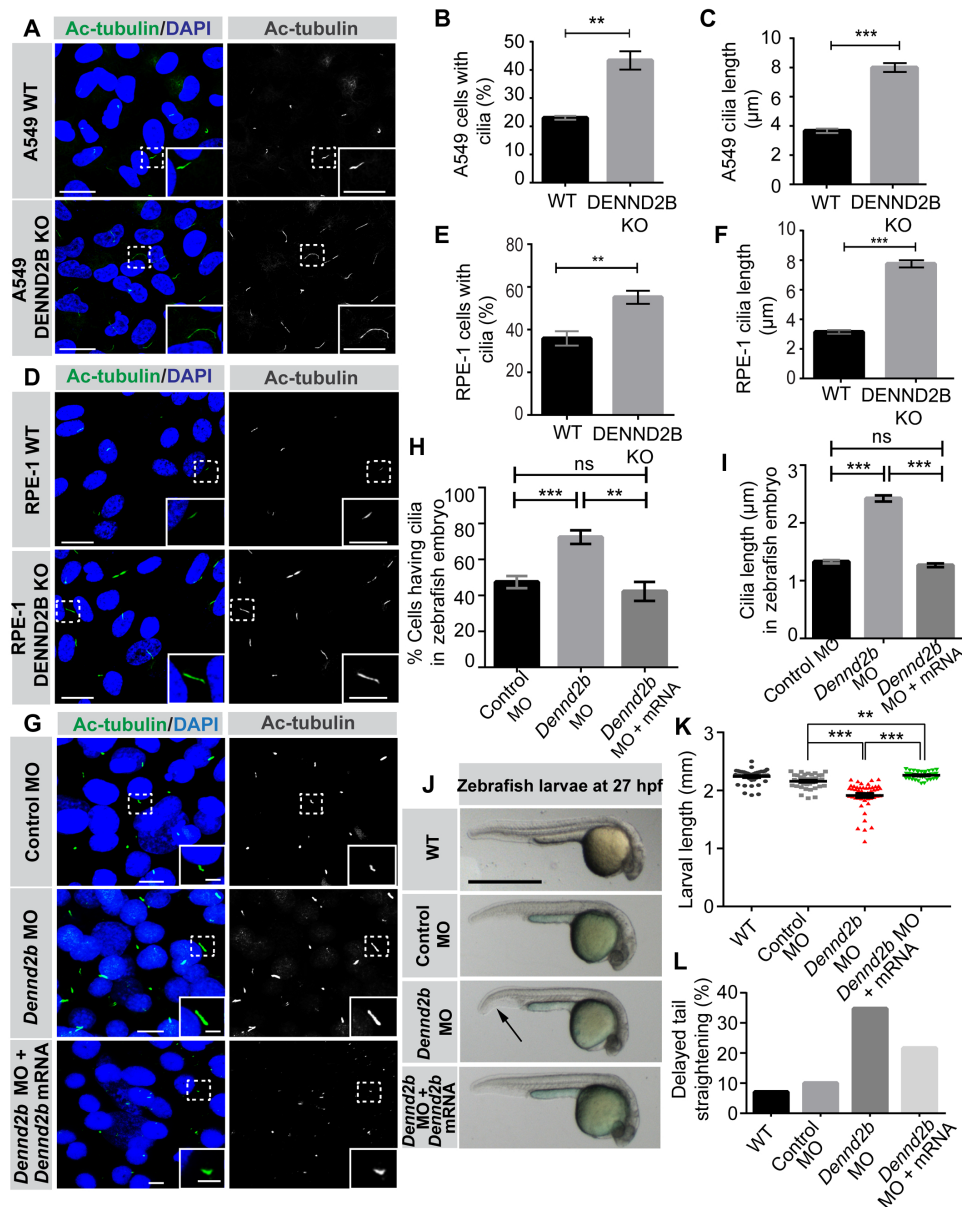
Fig. 4. Loss of DENND2B enhances primary cilia formation and cilia length. (**A**) Serum-starved A549 WT and DENND2B KO cells were fixed and stained with DAPI and Ac-tubulin antibody. Scale bars, 40 and 10 μm for the low- and high-magnification images, respectively. (**B** and **C**) Quantification of experiments as in (A); Mann-Whitney *U* test [>250 cells for (B) and 50 cells for (C)]. (**D**) Experiments were performed exactly as (A), except in RPE-1 cells. (**E**) Quantification of experiment in (D); unpaired *t* test (>250 cells). (**F**) Quantification of experiment as in (D); Mann-Whitney *U* test (<50 cells). (**G**) Zebrafish embryos at eight-somite stage injected with control or *DENND2B* MO or co-injected with *DENND2B* MO + *DENND2B* mRNA were stained with DAPI and Ac-tubulin antibody. Scale bars, 5 and 1.8 μm for the low- and high-magnification images, respectively. (**H**) Quantification of experiment as in (G); unpaired *t* test (>500 cells). (**I**) Quantification of experiment as in (G); Mann-Whitney *U* test (140 cells). (**J**) Example images of larval zebrafish at 27 hours post-fertilization (hpf). (**K**) Quantification of larval length; Kruskal-Wallis test, with pairwise multiple comparison (*n* = 42 for WT; *n* = 40 for control MO; *n* = 46 for *DENND2B* MO; *n* = 37 for *DENND2B* MO + *DENND2B* mRNA). (**L**) Percentage of larvae displaying delayed tail straightening. Means ± SEM. **$P < 0.01$ and ***$P < 0.001$

or a standard control MO oligonucleotide into the one-cell stage of zebrafish embryos. At the eight-somite stage, 13 hours post-fertilization (hpf), we labeled embryos with Ac-tubulin. Similar to phenotypes in the DENND2B KO cells, embryos injected with the *dennd2b* MO displayed an increased percentage of ciliated cells and enhanced cilia length (Fig. 4, G to I). At 27 hpf, we observed that *dennd2b* morphants were shorter in length and displayed a greater proportion

of a delayed tail-straightening phenotype compared to WT/control MO (Fig. 4, J to L). The phenotypes were rescued by the co-injection of DENND2B mRNA (Fig. 4, G to L). The larval length and tail phenotypes overlap with defects seen in other studies involving depletion of ciliary proteins in zebrafish, thus suggestive of a ciliopathy (*41*). Thus, DENND2B appears to play a role in development via regulation of primary cilia.

DENND2B inhibits primary cilia formation by functioning as a GEF for Rab10

Our screen reveals that the DENND2B DENN domain recruits Rab8, Rab10, and Rab35 to the mitochondria. Decreasing Rab8 function through expression of inactive Rab8 or depletion of the Rab8 GEF Rabin8 reduces cilia formation (*26*, *34*). Silencing of Rab35 does not alter cilia formation but decreases cilia length (*35*). DENND2B KO increases both the percentage of ciliated cells and cilia length. Thus, it is unlikely that either Rab8 or Rab35 are the mediators of the DENND2B activity. In contrast, the loss of Rab10 causes a significant increase in the percentage of ciliated cells (*36*) but does not alter cilia length (fig. S12, A to D). We thus sought to investigate the role of Rab10 in DENND2B-mediated ciliary phenotypes. Flag-DENND2B DENN domain efficiently immunoprecipitates the inactive form of Rab10 (T23N) but not the active form of Rab10 (Q68L) (fig. S13A), a hallmark of a GEF. Mutations in the catalytic site of the DENN domain of DENND2B, determined from the structure of Rab35-bound DENND1B (*42*, *43*), abolishes the recruitment of Rab10 to mitochondria (fig. S13B). An effector binding assay using a glutathione *S*-transferase (GST) fusion with a C-terminal fragment of MICAL-L2 (molecule interacting with CasL-like 2, also known as GST-MICAL-L2 C), which selectively binds the active form of Rab10 (*44*), reveals no changes in active Rab10 levels when we compared WT and DENND2B KO cells (fig. S13, C and D). This is not unexpected as other GEFs including DENND4C and Rabin8 are also known to function on Rab10 (*44*, *45*). We did however observe enhanced active Rab10 in lysates from cells transfected with GFP-DENND2B when compared with untransfected cell lysate (fig. S13, E and F), strongly supporting a GEF/substrate relationship for DENND2B and Rab10.

KO of DENND2B results in two distinct cilia phenotypes, enhanced cilia formation and increased cilia length. Overexpression of an active mutant of Rab10 (GFP-Rab10 Q68L) in DENND2B KO RPE-1 cells rescues the percentage of ciliated cells to a level similar to WT but does not rescue the enhanced cilia length phenotype (Fig. 5, A to C). This rescue is not seen with a nonprenylatable form of active Rab10 (GFP-Rab10 Q68L C_C del). Thus, membrane recruitment of active Rab10 is required for the rescue of the cilia formation phenotype resulting from DENND2B KO (fig. S14, A to C).

We next sought to examine the localization and dynamics of Rab10 relative to the primary cilia. GFP-Rab10 localizes at the ciliary base marked by γ-tubulin (fig. S15). Using fluorescence recovery after photobleaching (FRAP), we observed that green fluorescent protein (GFP)–Rab10 is rapidly recruited to the centriole (marked by centrin) after bleaching with a half-time of ~4.5 s (fig. S16, A to D). This could represent rapid vesicle trafficking of Rab10 to the centriole or recovery by recruitment from a cytosolic pool. Analysis of the localization of endogenous Rab10 using a KO-validated antibody revealed a bright puncta located exclusively to the mother centriole marked by partial overlap with CEP164 (Fig. 5, D and E), consistent with the localization of DENND2B.

Given that Rab10 inhibits cilia growth, we predicted that induction of ciliogenesis would remove Rab10 from the base of the cilia. WT and DENND2B KO A549 cells were serum-starved and stained for Ac-tubulin and endogenous Rab10. While endogenous Rab10 staining at the mother centriole was obvious in most growing WT cells (Fig. 5, D and E), upon serum starvation, a subtle (~9%) but significant percentage of WT cells had Rab10 puncta at the base of primary cilia (Fig. 5, F to H), suggesting that most cells had lost Rab10 from the basal body. In contrast, we did not observe a single

DENND2B KO cell with Rab10 puncta at the base of primary cilia (Fig. 5, F and G), consistent with the idea that GEFs control the localization of Rabs (*46*) and that the loss of DENND2B disrupts Rab10 localization. Subsequently, expression of GFP-DENND2B in the KO cells resulted in ~8% of cells showing Rab10 staining at the ciliary base (fig. S17, A and B). In addition, we also demonstrate that GFP-DENND2B (~1.5-fold overexpression; fig. S18B) and Rab10 colocalize proximal to CEP164 (fig. S18A). Together, these data suggest that DENND2B activates Rab10 and that activated Rab10 localized at the mother centriole controls primary cilia formation.

DENND2B controls cilia length by activating RhoA

Following DENND2B KO, expression of Rab10 rescues defects in the percentage of ciliated cells (Fig. 5B) but does not rescue defects in cilia length (Fig. 5C). We thus sought to understand the mechanism by which DENND2B controls cilia length. The physiological need for primary cilia of a defined length is not clear, but a genetic mutation altering cilia length represses Hh signaling (*47*). Consistently, as monitored by the expression of the Gli1 transcription factor (*48*, *49*), Hh signaling is repressed in the absence of DENND2B (fig. S19). Activation of RhoA has been linked to cilia length, specifically, cells with higher levels of active RhoA have shorter cilia, possibly through the formation of stress fibers (*50*, *51*), whereas reduced RhoA activity leads to longer cilia (*52*). We thus considered that DENND2B could control cilia length by acting as a GEF for RhoA. DENN(2B) relocates RhoA to the mitochondria, inducing gross morphological changes (Fig. 6A). The GEF dead mutant of DENN(2B) does not recruit RhoA, reinforcing that catalytic activity of the DENN(2B) is required for mitochondrial recruitment (Fig. 6A). Mitochondrial recruitment of RhoA is independent of Rab10 and occurs as normal in the absence of endogenous Rab10 (fig. S20, A and B). We next measured levels of active RhoA in DENND2B KO cells using GST fused to the Rho-binding domain (RBD) of the effector protein Rhotekin, which selectively recognizes cellular RhoA in the active, GTP-bound form (*53*). There is a significant decrease in active RhoA in DENND2B KO cells as compared to WT cells, whereas total RhoA remains unchanged (Fig. 6, B and C). Conversely, overexpression of DENND2B increases the levels of active RhoA (Fig. 6, D and E). In coimmunoprecipitation experiments, DENND2B interacts preferentially with inactive RhoA (T19N) as compared to active RhoA (Q63L) (Fig. 6F), a hallmark of GEFs. Thus, the substrates of DENN domains may now be expanded beyond Rab GTPases.

We next asked whether increasing the levels of GTP-loaded RhoA could rescue the cilia length phenotype resulting from DENND2B KO. RhoA activation using CN03 restored cilium length to normal in DENND2B KO A549 cells as did the expression of active RhoA (RhoA: ~1.5-fold; Fig. 7, A to C, and fig. S21). RhoA activation by CN03 in DENND2B KO cells overexpressing active Rab10 (GFP-Rab10 QL; Rab10: ~2-fold; fig. S21) rescued both the percentage of ciliated cells and ciliary length (Fig. 7, A to C) as did coexpression of both active GTPases (fig. S22, A and B). Thus, DENND2B controls cilia length by controlling the GTP status of RhoA and the percentage of ciliated cells by controlling the GTP status of Rab10.

DENND2B controls recruitment of CP110 via Rab10

Proteins critical for negative regulation of primary cilia formation are CP110 and its interacting partner centrosomal protein of 97 kDa (CEP97) (*54*). CP110 is recruited by binding to CEP97 at the distal
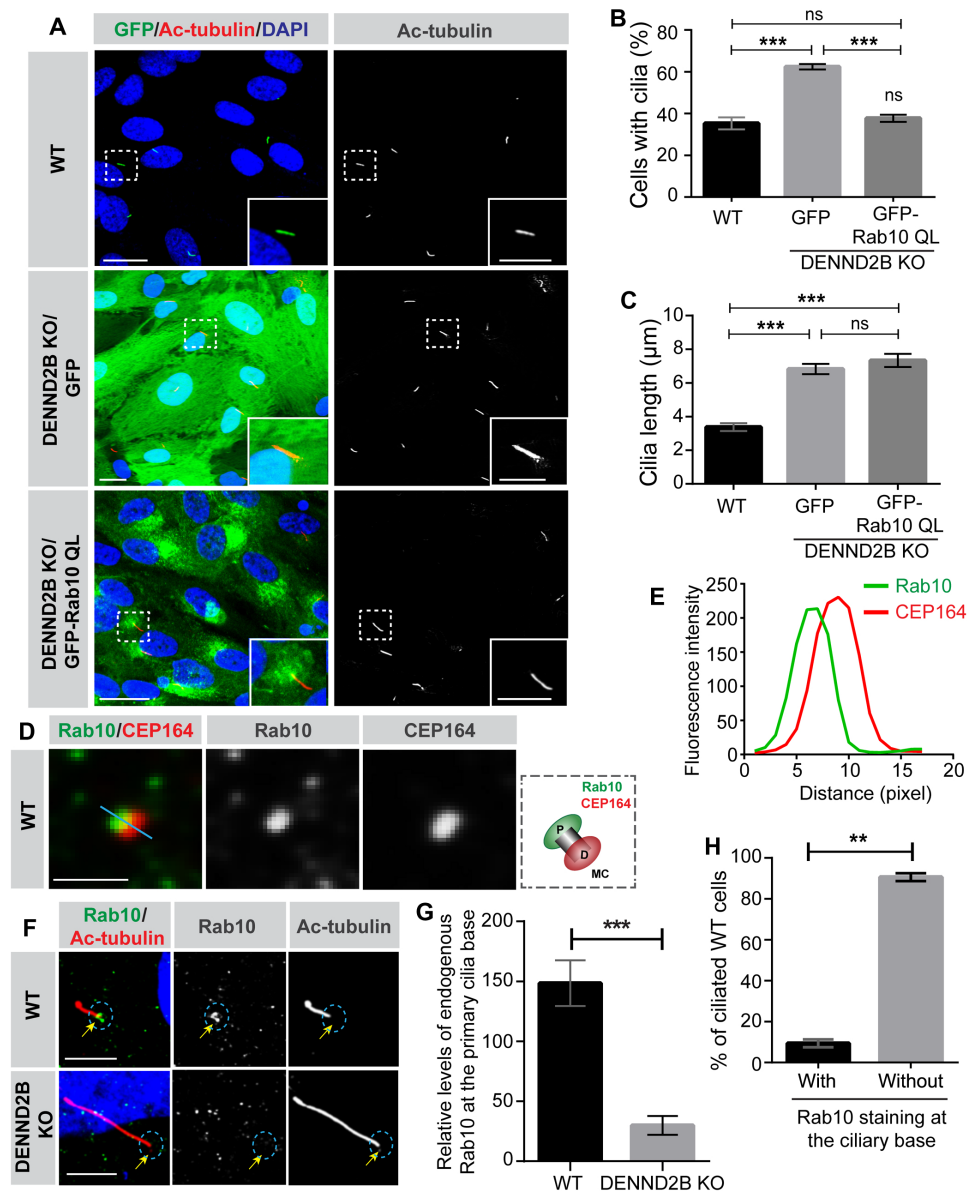
Fig. 5. Active Rab10 rescues defects in primary cilia formation but not length. (**A**) RPE-1 cells expressing GFP or GFP-Rab10 QL (active mutant) were starved and stained with Ac-tubulin antibody to mark primary cilia. Scale bars, 20 and 10 μm for low- and high-magnification images, respectively. (**B** and **C**) Quantification of experiments as in (A); means ± SEM; one-way analysis of variance (ANOVA), with Tukey's posttest (***$P < 0.001$). $n > 250$ cells for (B) and 50 cells for (C). (**D**) Unstarved A459 WT cells were stained with Rab10 and CEP164 antibodies to reveal the mother centriole. Scale bar, 1.2 μm. (**E**) Intensity profiles along the straight blue line in (D). (**F**) Starved A549 cells were stained with Rab10 and Ac-tubulin antibodies for primary cilia (red). Scale bars, 5.5 μm. The yellow arrows in (F) represent the base of cilia (stained with anti–Ac-tubulin antibody). (**G**) Quantification of experiments as in (F). Means ± SEM; unpaired t test (***$P < 0.001$; $n = 5$). (**H**) Quantification of experiments as in (F); means ± SEM; Mann-Whitney U test (**$P < 0.01$; $n > 50$).

ends of both the mother and daughter centrioles (*54*). Upon serum starvation or in the G_0 phase, CP110 uncapping from the distal end of the mother centriole is required for it to mature into a basal body and initiate primary cilia formation (*39*). However, the mechanisms regulating CP110 recruitment are not fully understood.

γ-Tubulin marks the centriolar region containing the mother and the daughter centrioles. In the absence of DENND2B, only ~5% of A549 cells had both mother and daughter centrioles capped with CP110 (two dots) as compared to WT cells where ~50% of the cells had both centrioles capped (Fig. 8, A and B). We next analyzed the

capping of CP110 specifically at the distal end of the mother centriole. A significantly smaller proportion of DENND2B KO cells had CP110 localized at the distal appendage of the mother centriole, as marked by CEP164 (Fig. 8, C and D). These results demonstrate that DENND2B sets up a permissive environment for the accumulation of CP110 to the distal end of the mother centriole as a mechanism to control capping status and primary cilia formation.

We next sought to determine whether Rab10 functions downstream of DENND2B in the capping function of CP110 at the mother centriole. An active mutant of Rab10 is located at the mother
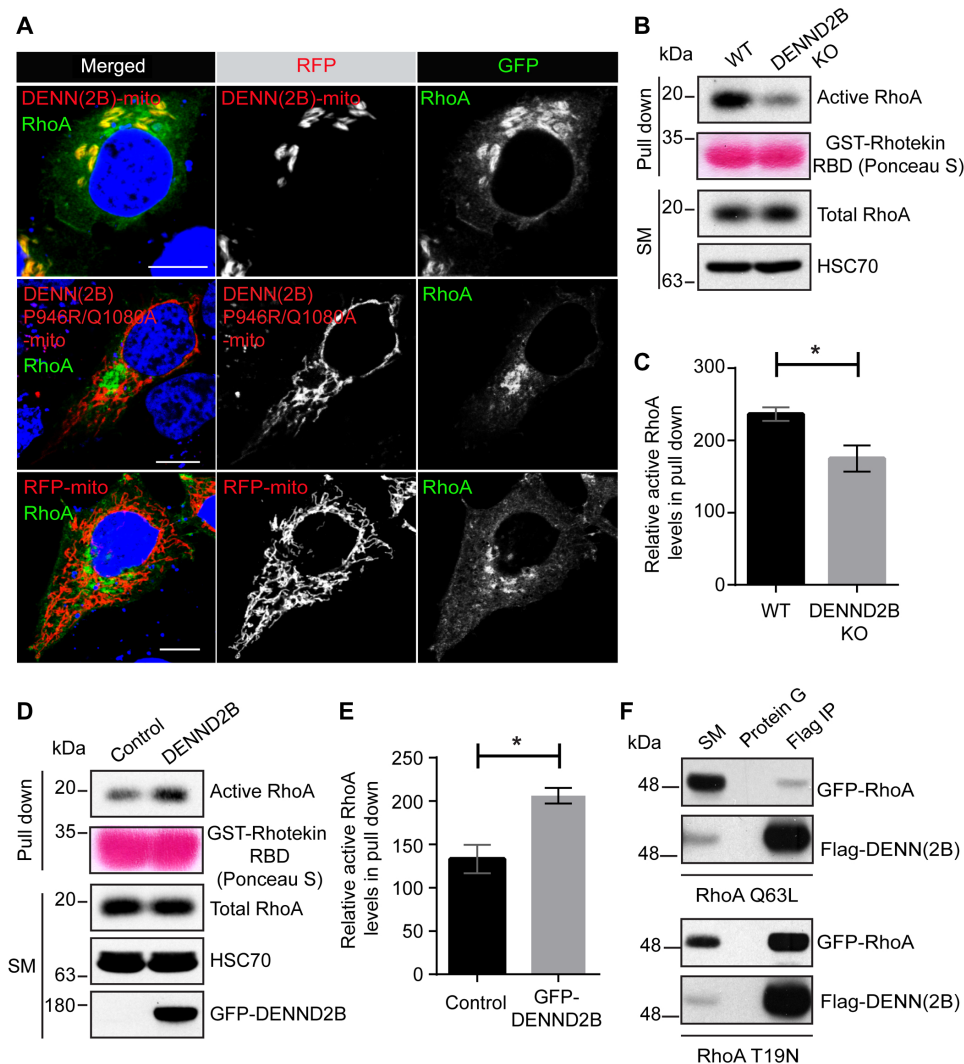
Fig. 6. The DENND2B DENN domain binds RhoA and functions as a RhoA GEF. (A) HeLa cells cotransfected with GFP-RhoA WT and DENN(2B)-mito, DENN(2B)-mito with double mutations P946R/Q1080A predicted to inhibit GEF activity, or RFP-mito that were fixed and stained with DAPI (blue) to reveal nuclei. Scale bars, 10 μm. **(B)** WT or DENND2B KO A549 cell lysates were incubated with purified GST-Rhotekin RBD protein. Specifically bound proteins were detected by immunoblot with anti-RhoA antibody. The starting material (SM) was run in parallel to detect the total RhoA. Anti-HSC70 antibody was used as a loading control. **(C)** Quantification of experiment in (B); means ± SEM; unpaired t test (*$P \leq 0.05$; $n = 3$). **(D)** HEK-293T cells were transfected with GFP-DENND2B. At 24 hours post-transfection, transfected or untransfected (control) cell lysates were incubated with purified GST-Rhotekin RBD. Specifically bound proteins were detected by immunoblot with anti-RhoA antibody or anti-GFP antibody recognizing DENND2B or anti-HSC70 antibody for loading control. **(E)** Quantification of experiment in (D); means ± SEM; unpaired t test (*$P \leq 0.05$; $n = 3$). **(F)** HEK-293T cells were cotransfected with Flag-DENN(2B) and GFP-RhoA T19N or GFP-RhoA Q63L. At 24 hours post-transfection, cells were lysed and incubated with protein G–agarose alone (mock) or protein G–agarose with anti-Flag antibody (Flag IP). Specifically bound proteins were detected by immunoblot with anti-GFP antibody to detect active/inactive Rab10 or anti-Flag antibody recognizing DENN(2B).

centriole marked by CEP164 (Fig. 8, E and F) and in DENND2B KO cells, where CP110 no longer caps the mother centriole, expression of GFP-tagged active Rab10 restores recruitment of CP110 to the mother centriole seen by colocalization with γ-tubulin (Fig. 8, G and H). Furthermore, in coimmunoprecipitation experiments, CP110 binds to both the active and inactive mutants of Rab10 (fig. S23). Because it is the membrane-bound active form of Rab10 that rescues the formation of cilia, we propose that DENND2B-mediated activation of Rab10 drives the recruitment of CP110 to the mother centriole.

Rab10 functions in Parkinson's disease associated with autosomal dominant mutations in the leucine-rich repeat kinase 2 (LRRK2) gene. Dominant mutations in LRRK2 autoactivate the LRRK2 kinase, which phosphorylates active Rab10 (*36*, *55*, *56*). Phospho-Rab10 (p-Rab10) localizes to the mother centriole, where it blocks the release of CP110 and inhibits cilia formation (*36*, *57*). We thus investigated the levels of p-Rab10 in A549 cells as they contain high levels of WT LRRK2. We did not find any changes in overall p-Rab10 levels between A549 WT and DENND2B KO cells (fig. S24A), which is not unexpected as DENND2B KO had no influence on the overall active Rab10 levels (fig. S13, C and D). However, we did find an increase in p-Rab10 levels in cell lysates overexpressing WT LRRK2 and DENND2B when compared to cell lysates overexpressing WT LRRK2 alone, indicating that LRRK2 phosphorylates active Rab10 after activation by DENND2B (fig. S24B).
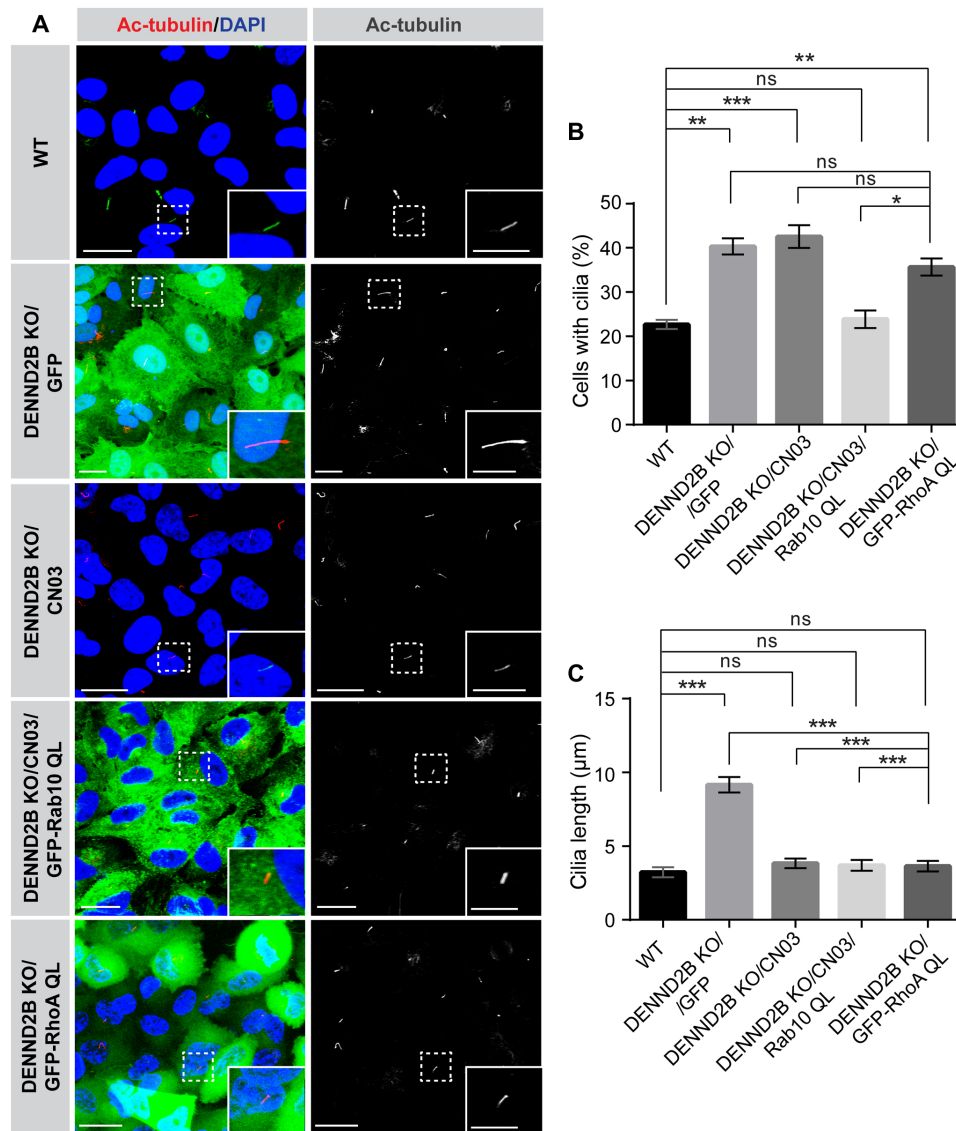
Fig. 7. Overexpression of active RhoA mutant in DENND2B KO cells restores normal cilia length but not primary cilia formation. (**A**) DENND2B KO A549 cells were transduced with lentivirus driving overexpression of either GFP alone, GFP-RhoA QL (active mutant), or GFP-Rab10 QL (active mutant). The cells were then treated or not treated with CN03 as indicated. All cells were then serum-starved for 24 hours and were then fixed and stained with DAPI to reveal nuclei and Ac-tubulin antibody for primary cilia (red). Scale bars, 20 μm for the low-magnification images and 10 μm for the higher-magnification insets. (**B**) Quantification of percentage of ciliated cells as shown in (A); means ± SEM; one-way ANOVA, with Tukey's posttest (***$P \leq 0.001$, **$P \leq 0.01$, and *$P \leq 0.05$; $n > 250$ cells per condition). (**C**) Quantification of the ciliary length as shown in (A); means ± SEM; Kruskal-Wallis test, with pairwise multiple comparison posttest (***$P \leq 0.001$; $n > 20$ cells per condition).

In addition, treatment of A549 cells with the LRRK2 inhibitor MLI-2 reduced p-Rab10 levels, demonstrating that phosphorylation of Rab10 is mediated by LRRK2 (fig. S24A). Thus, it is possible that DENND2B-activated Rab10 is phosphorylated by LRRK2 to inhibit cilia formation.

DISCUSSION

The identification of GEFs for Rab GTPases is critical for understanding membrane trafficking and, by extension, the pathophysiology of multiple human diseases. Most mammalian Rabs have no assigned GEF. Here, we use a cell-based GEF assay to screen for all Rab substrates of the seven members of the DENND1 and DENND2 DENN domain–containing protein subfamilies. The large number of substrates identified were not seen using more traditional in vitro approaches. The most important advantage of the cell-based system is that the Rab substrates have all of the cellular requirements to retain their endogenous nucleotide status, something that is often lost following their purification. However, the degree of overexpression of both the GEFs and the Rab substrates may drive lack of specificity even in cells. For example, DENND4C is present in multiple cell lines at very low levels and yet it is a potent GEF for Rab10 (*45*). In addition, we cannot rule out that some of the identified Rabs are recruited to mitochondria as part of Rab cascades downstream of true Rab substrates. Given the unexpected diversity of Rab substrates for the seven DENN domains tested, our approach
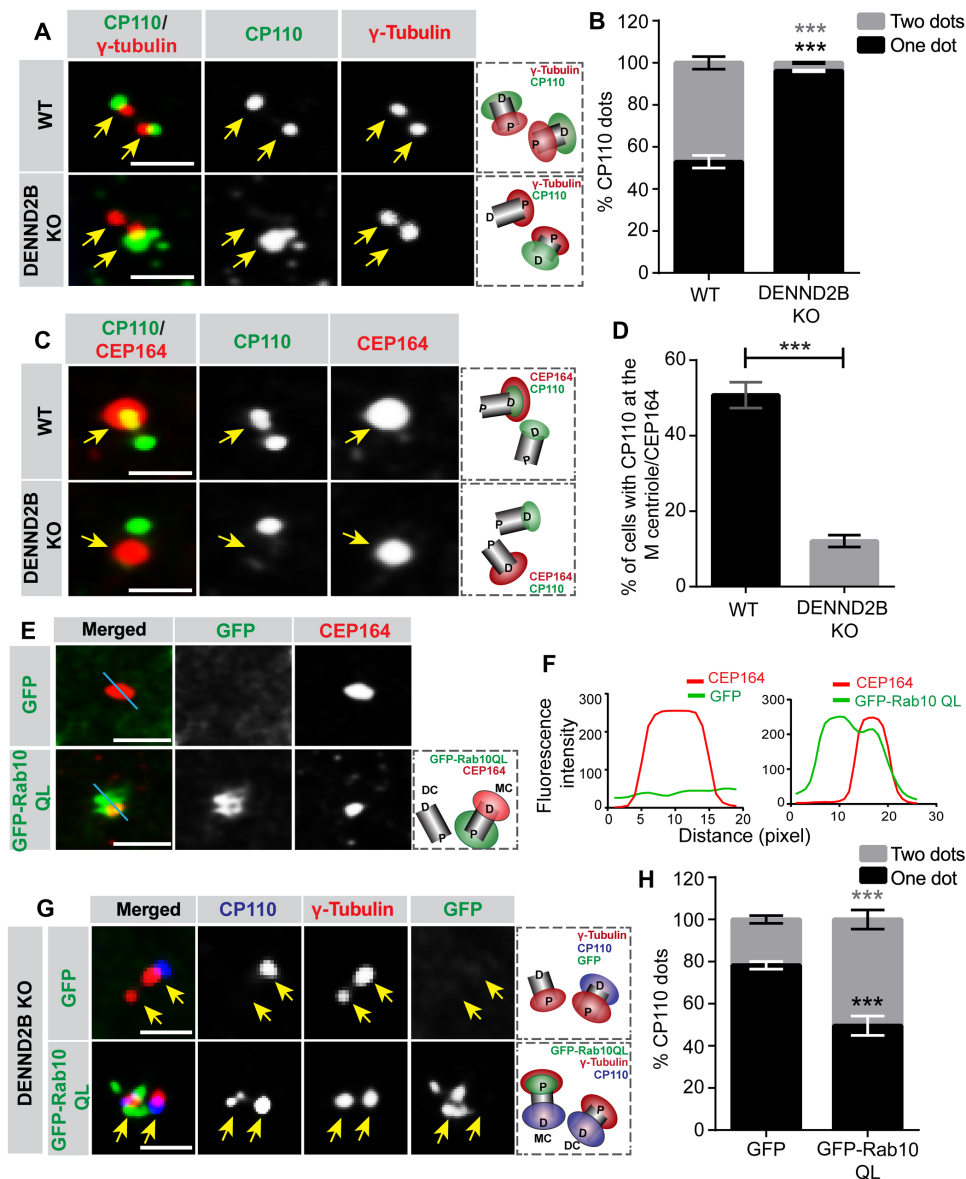
Fig. 8. Inactivation of Rab10 impairs recruitment of CP110 to the mother centriole. (**A**) A549 cells were starved and stained with CP110 and γ-tubulin antibodies. Scale bars, 1.57 μm (**B**) Quantification of experiments as in (A); means ± SEM; unpaired *t* test (***$P \leq 0.001$; $n > 70$ cells per condition). (**C**) Cells as in (A) were stained with CP110 and CEP164 antibodies. Scale bars, 1.4 μm (**D**) Quantification of experiments as in (C); means ± SEM; unpaired *t* test (***$P \leq 0.001$; $n > 90$ cells per condition). (**E**) A549 cells expressing GFP or GFP-Rab10 QL were starved and stained with CEP164 antibody for mother centriole. Scale bars, 2.10 μm. (**F**) Intensity profiles along the straight blue lines from the image in (E). (**G**) A549 cells expressing GFP or GFP-Rab10 QL were stained with CP110 and γ-tubulin antibodies for centrioles. Scale bars, 1.1 and 1.7 μm for GFP and GFP-Rab10 QL, respectively. (**H**) Quantification of experiments as in (G); means ± SEM; unpaired *t* test (***$P \leq 0.001$; $n > 45$ cells per condition).

likely explains why there are far fewer GEFs compared to the total number of Rab GTPases (*14*).

In addition to confirming four known DENN/Rab pairs, we identify 19 novel pairs: DENND1A/B/C with Rab15; DENND2A with Rab15; DENND2B with Rab8A, Rab8B, Rab10, Rab15, Rab27A, Rab27B, and Rab35; DENND2C with Rab8A, Rab8B, Rab10, Rab15, and Rab35; and DENND2D with Rab8A and Rab10. This indicates that individual DENN families are not selective for a single Rab. Of all the newly identified Rab GTPases, only Rab8A, Rab8B, Rab10, Rab13, and Rab15 have a strong phylogenetic correlation belonging to one subfamily (*2*), suggesting no specific phylogentic pattern in

regard to pairs identified in association with the DENND1 and DENND2 families. Furthermore, although both Rab8A and Rab8B were identified as substrates for DENND2B and DENND2C, only Rab8A and not Rab8B was identified with DENND2D, despite very high sequence similarity. Thus, there is a high degree of specificity inherent in the screen and in DENN domain recognition of substrates. In contrast, all but one of the DENN domains screened activated Rab15, suggesting a certain promiscuity that could function to enhance combinatorial possibilities in cell signaling events. While most members of the DENND2 family are not well studied, we now know that all members of the DENND1 family activate

Rab35 at different cellular locations. DENND1A and DENND1B are largely restricted to the endocytic system, whereas DENND1C is associated with the actin cytoskeleton (*17*). Another possibility is tissue-specific functions of the DENN domain proteins. For example, a cascade of Rabs (Rab35, Rab8A, and Rab13) and effector proteins (MICAL-L1/L2) controls neurite outgrowth (*58*). Given that DENND2B interacts with MICAL-like proteins (*19*), it would be worth investigating whether DENND2B plays a role in such signaling mechanisms.

Several Rab GTPases have been associated with primary cilia, either in stimulatory or inhibitory roles (*21*). Here, we demonstrate that Rab10 is a physiologically relevant substrate of DENND2B and that DENND2B activates Rab10 to inhibit primary cilia formation. Furthermore, we found that Rab10 controls recruitment of CP110, a repressor of ciliogenesis, at the distal appendage of the mother centriole, thereby explaining the inhibition of cilia formation (Fig. 9A).

The extracellular pathway for ciliogenesis involves docking of the basal body with the plasma membrane with formation of cilia from the surface. In contrast, the intracellular pathway requires ciliary vesicles derived from the Golgi to encapsulate the mother centriole at an early stage of cilia formation within the cytoplasm (*24*, *25*). Subsequently, accumulation of ciliary vesicles forms a double-membrane sheath around the basal body (matured mother centriole), and the growing axonemal microtubules form a nascent intracellular cilium, which then migrates and fuses with the plasma membrane, exposing the cilium to the external environment (*24*). Rab10 and DENND2B are involved in the trafficking of endosomal/Golgi vesicles to the plasma membrane (*31*). While it is unclear how DENND2B is recruited to the proximal end of the mother centriole, we propose that DENND2B activates and recruits Rab10 that

further recruits CP110 to the mother centriole, and it is the recruitment of CP110 to the distal end of the mother centriole that prevents the maturation of the mother centriole to the basal body and ultimately cilia formation.

Two independent studies provide evidence that the nucleotide status of RhoA controls cilia length (*50*, *52*). In addition, high levels of active RhoA induce the formation of stress fibers that prevent primary cilia outgrowth (*51*). Although nearly 80 RhoGEFs are known to regulate signaling events (*59*), none have been linked to ciliogenesis. We now demonstrate that DENND2B activates RhoA and controls cilia length, and we provide compelling evidence that DENND2B is a GEF for RhoA (Fig. 9B). Last, overexpression of active RhoA mutant reverses normal cilia length resulting from DENND2B KO. Thus, the substrates for DENN domain proteins must be expanded beyond Rab GTPases. Although we provide evidence of DENND2B functioning as a GEF for RhoA using the mitochondrial recruitment assay and other standard protocols for the identification of Rho GEFs (*60*, *61*), we cannot rule out the possibility of another Rab getting recruited by DENND2B, which further recruits RhoA through a GTPase cascade.

In addition, our analysis reveals that Hh signaling is suppressed in DENND2B KO cells. Any alteration in Hh signaling is known to cause a diverse spectrum of disorders, known as primary ciliopathies (*62*). A patient with a DENND2B loss-of-function mutation presents a diverse set of severe anomalies related to ciliopathies (*27*, *32*), and it is likely that defects in primary cilia contribute to the disease phenotype. Knockdown of *dennd2b* in zebrafish reveals reduced larval length and a curved tail along with ciliary defects, indicating that dennd2b-mediated regulation of primary cilia might be contributing to the developmental defects. KO mice for M-phase
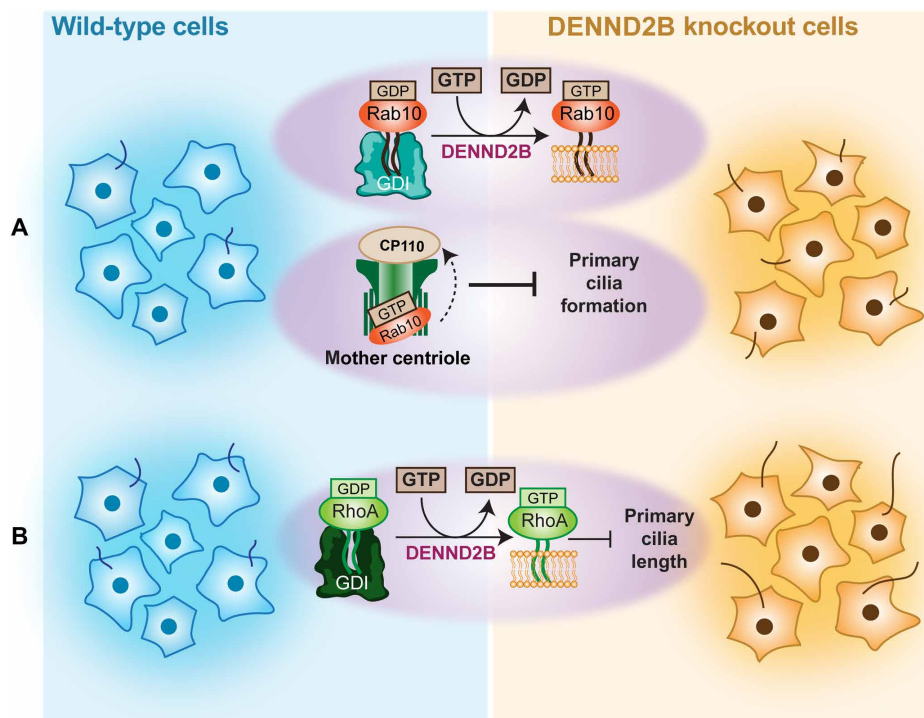

Fig. 9. Model of DENND2B regulating primary cilia. (**A**) Schematic representation of DENND2B regulating primary cilia via activation of Rab10. (**B**) DENND2B activating RhoA and controlling primary cilia length.

phosphoprotein 9 (MPP9), a protein involved in the recruitment of CP110 to the mother centriole, also showed decreased body weight/length and a twisted body axis at midgestation (63), suggesting that DENND2B and MPP9 may be part of a common pathway. DENND2B recruits multiple other Rabs to the mitochondria (Rab8A/B, Rab15, Rab35, and Rab27A/B), and therefore signaling mechanisms governed by the remaining GTPases are yet to be found.

An intriguing question relates to how multiple DENN domains can target a single Rab and how the same DENN domain can target multiple Rabs. This may be explained, in part, by different DENN domain proteins acting on a common Rab but at different subcellular compartments. For example, DENND1A/B activates Rab35 at endosomes, whereas DENND1C activates Rab35 at the actin cytoskeleton (17). For Rab10, there are multiple GEFs including DENND2C and DENND2D, newly demonstrated in this study, and DENND4C (45) and Rabin8 (44). It is possible that all GEFs are present in any given cells but that they activate Rab10 at different subcellular locations. When we performed KO of DENND2B, we saw no change in the total cellular levels of the active form of Rab10, likely due to the presence of multiple other Rab10 GEFs. Immunofluorescence analysis indicates that the pool of Rab10 at the centriole is a relatively minor component of the overall cellular pool of Rab10. This further stresses that DENND2B selectively activates Rab10 to function at the centriole. In addition, the answer for the broad diversity in substrate specificity within and between families could be unveiled once we solve the structure of the individual DENN domains. While we have screened two major families of DENN domains in this manuscript, all the remaining DENN domain family members must be screened using a similar approach to understand the full complement of substrates. Because DENN domains are no more specific for Rabs, they must be screened across all the small GTPase families in the future.

As our study finds new aspects of DENN domains in membrane trafficking, it also poses several questions related to DENND2B. DENND2B is known to promote cancer invasion (19). Coincidently, numerous cancer cells lack primary cilia (64). Given the inhibitory role of DENND2B in primary cilia, is it possible that the disrupted function of DENND2B gives rise to cancer phenotypes via defective primary cilia? In addition, previous studies have reported that Rab8A and Rab10 have opposite effects on cilia formation. Because both Rab8A and Rab10 are substrates for DENND2B, it will be important to investigate factors contributing to context-specific GEF activity that leads to Rab10-specific phenotype but not Rab8A. The Parkinson's disease gene LRRK2 phosphorylates a subset of Rabs (65). Of all the Rabs, Rab10 has been recently associated with an emerging Parkinson's disease cellular phenotype, inhibition of primary cilia formation by p-Rab10 (36). Note that overexpression of DENND2B increases the levels of Rab10 phosphorylated by LRRK2. DENND2B KO cells show increased cilia formation, and reduced p-Rab10 fits the model published by other groups showing that increased LRRK2-mediated phosphorylation of Rab10 inhibits cilia formation (36, 57). This finding raises important questions that need further investigation: (i) Does DENND2B interact with LRRK2 to modulate its activity and, if so, under what circumstances? (ii) Does DENND2B function upstream of LRRK2 in known cell biological events such as in macropinocytosis to mediate immunological responses in phagocytes (66)?

In summary, we demonstrate that DENN domains have a wide spectrum of GTPase substrates, even outside the Rab family. More specifically, we have uncovered DENND2B as a GEF localized at the base of the primary cilia, negatively regulating primary cilia formation and ciliary length by controlling activation of Rab10 and RhoA. In addition, with the DENND2B zebrafish showing developmental defects, a thorough analysis must be performed to understand the impact of Hh signaling, with the possibility of extending the analysis to mice. Last, it is still unanswered as to how DENND2B is inhibited under normal physiological conditions to allow primary cilia formation. Understanding the DENN/GTPase-mediated complex trafficking mechanisms will have potential implications in multiple disease paradigms, from developmental disorders to neurodegeneration and cancer.

MATERIALS AND METHODS
Cell lines
Human embryonic kidney (HEK) 293T, HeLa, A549, and RPE-1 cells were from the American Type Culture Collection (CRL-1573, CCL-2, CCL-185, and CRL-4000).

Cell culture
All cell lines were cultured in Dulbecco's Modified Eagle's medium (DMEM) high-glucose (GE Healthcare, catalog no. SH30081.01) containing 10% bovine calf serum (GE Healthcare, catalog no. SH30072.03), 2 mM L-glutamate (Wisent, catalog no. 609065), 100 IU of penicillin, and streptomycin (100 μg/ml) (Wisent, catalog no. 450201). Serum starvation media are as follows: DMEM high-glucose containing 2 mM L-glutamate, 100 IU of penicillin, and streptomycin (100 μg/ml). Cell lines were routinely tested for mycoplasma contamination using the mycoplasma detection kit (biotool, catalog no. B39038).

DNA constructs
GST-MICAL-L2-C and all 60 GFP-Rab constructs were gifts from M. Fukuda (Tohoku University) (44, 67–69). RFP-mito was generated, replacing venus in mVenus-N1 vector (table S1). DENN(1A)-mito, DENN(1B)-mito, DENN(1C)-mito, DENN(2A)-mito, DENN(2B)-mito, DENN(2C)-mito, and DENN(2D)-mito were cloned into RFP-mito. Lenti GFP-Rab10 Q68L construct was generated using the QuickChange lightning site-directed mutagenesis kit (Agilent Technologies) on lentivirus vector pSLQ1371 containing GFP-Rab10 (36). GFP lentivirus construct was generated by subcloning GFP in pLVX-M-Puro vector at Xho I and Xba I sites by Synbio Technologies. Plasmids from Addgene are as follows: GFP-RhoA Q63L (Addgene, 12968), GFP-RhoA T19N (Addgene, 12967), 2XMyc-LRRK2-WT (Addgene, 25361), GFP-Rab10Q68L (Addgene, 49544), GFP-Rab10T23N (Addgene, 49545), dTomato-centrin-1 (Addgene, 73332), and pMito-mCherry-FRB (Addgene, 59352). Lenti GFP-RhoA Q63L was cloned into pLVX-M-puro vector (Addgene, 125839). Amplified insert of the coding sequence of Rab35 having double-cysteine residues deleted at the C terminus was cloned into the pEGFP-C1 vector. GST-Rhotekin RBD (murine 7 to 89) was obtained from M. Olson. GFP-DENND2B, mCh-DENND2B, and Flag-DENN(2B) were described previously (19). Human CP110 (GenBank, BC036654.2) was synthesized and subcloned into pCMV-tag2B vector by Synbio Technologies. GFP or GFP-DENND2B was subcloned into pLVX-M-puro vector by Synbio Technologies. Flag-CP110 was synthesized by SynBio. Successful cloning of constructs were verified by sequencing. Refer to table S1 for cloning strategies and oligo sequences.

Generation of DENND2B KO line (A549 and RPE-1)

Two guide RNAs (gRNAs) (Target_1-318: CGTCTCTCTTGCAC-GCCGAA; Target_2-442: CGGGTCAGCAAGACGCCCCG) were obtained from Applied Biological Materials and separately cloned into pLenti-U6-sgRNA-SFFV-Cas9-2A-Puro to increase the chances of generating a KO line. Lentivirus-based delivery of gRNA and Cas9 was used to KO *DENND2B* from A549 and RPE-1 cells. One 15-cm plate containing 10^7 HEK-293T cells were transfected with 7.5 μg of each gRNA constructs, 15 μg of psPAX2 (obtained from S. Pfeffer), and 7.5 μg of pMD2 VSV-G (obtained from S. Pfeffer) using calcium phosphate. At 8 hours post-transfection, the culture medium was replaced with collection medium [15 ml per plate; regular medium supplemented with 1× nonessential amino acids (Gibco) and 1 mM sodium pyruvate (Gibco)]. The medium was collected at 24 and 36 hours and replaced with fresh medium (15 ml per plate) with each collection. The collected medium at 24 hours was stored at 4°C until the last collection. The collected culture media were then filtered through a 0.45-μm α-polyethersulfone (PES) membrane. A total of 5×10^4 A459 and RPE-1 cells were seeded in one well of a 24-well plate. The next day, regular culture media were replaced with the filtered supernatant containing lentivirus (2 ml each well) and incubated for 48 hours. Following incubation, puromycin-resistant cells were selected with puromycin (2.5 μg/ml) in the culture medium for 48 hours. After selection, cells were isolated by clonal dilution. Following the expansion of selected colonies, KOs were confirmed by sequencing of the PCR-amplified genomic DNA.

Transfection

HeLa, A549, and RPE-1 cells were transfected using the jetPRIME Transfection Reagent (Polyplus) according to the manufacturer's protocol. HEK-293T cells were transfected using calcium phosphate.

Small interfering RNA–mediated knockdown of Rab10

HeLa cells were plated at ~80% confluency. Cells were transfected using Lipofectamine RNAiMax (catalog number: 13778-150) from Thermo Fisher Scientific according to the manufacturer's guidelines and were used 48 hours after knockdown. Control small interfering RNA (siRNA) (ON-TARGETplus; D-001810-10-20) and Rab10 siRNA-targeting genome pool (SMARTpool:ON-TARGETplus; L-010823-00-0010) were purchased from Dharmacon/Horizon Discovery.

Antibodies and reagents

Mouse monoclonal Flag (M2) antibody is obtained from Sigma-Aldrich (F3165). Rabbit polyclonal GFP (A-6455) is obtained from Invitrogen, and rat monoclonal HSC70 antibody [Western blot (WB)-1:10,000] is from Enzo (ADI-SPA-815-F). Alexa Fluor 488– and Alexa Fluor 647–conjugated rabbit secondary antibodies are from Invitrogen. Purified anti-calnexin antibody (W17077C) is from BioLegend [immunofluorescence (IF)-1:1000], anti-PMP70/ABCD3 antibody (sc-514728) is from Santa Cruz Biotechnology (IF-1:500), anti-CP110 antibody (methanol fixation; IF-1:100) is from Proteintech (12780–1-AP), anti-CEP164 antibody (methanol/paraformaldehyde fixation, IF-1:100) is from Santa Cruz Biotechnology (sc-515403), anti-LAMP1 antibody (IF-1:200) is from Cell Signaling Technology (D2D11), anti-TOM20 antibody (IF-1:500) is from Abcam (ab186734), anti-EEA1 antibody (IF-1:100) is from BD Transduction Laboratories (610456), anti-GM130 antibody (IF-1:500) is from BD Transduction Laboratories (610822), anti-Rab10 antibody (WB-1:1000) is from Cell Signaling Technology (D36C4), anti-Rab10 antibody (IF-1:1000) is from Abcam (ab237703), anti–p-Rab10 antibody (WB-1:1000) is from Abcam (ab230261), anti-LRRK2 antibody (WB-1:1000) is from Abcam (ab133518), anti-RhoA antibody (WB-1:1000) is from Cell Signaling Technology (67B9), anti–Ac-tubulin antibody (IF-1:1000) is from Cell Signaling Technology (D20G3), anti-DENND2B antibody (WB-1:1000) is from GeneTex (GTX55282), anti–γ-tubulin antibody (1:100) is from Sigma-Aldrich (T6557), and MLI-2 is from Tocris Bioscience (5756).

Lentivirus production

For each virus, 10 cm by 15 cm plate containing 10^7 HEK-293T cells were transfected with 30 μg of lenti construct containing protein of interest, 30 μg of psPAX2, and 15 μg of pMD2 VSV-G using calcium phosphate. At 8 hours post-transfection, the culture medium was replaced with collection medium (15 ml per plate; regular medium supplemented with 1× nonessential amino acids and 1 mM sodium pyruvate). The medium was collected at 24 and 36 hours and replaced with fresh medium (15 ml per plate) with each collection. The collected medium at 24 hours was stored at 4°C until the last collection. The collected culture media were then filtered through a 0.45-μm PES membrane and concentrated by centrifugation (16 hours at 7000 rpm), and the resulting pellets were resuspended in DMEM in 1/5000 of the original volume. Concentrated viruses were aliquoted and stored at −80°C until use.

Protein overexpression using lentivirus

Concentrated lentivirus was added to the cells with minimum culture media (for example, 200 μl of the medium for each well in a four-chambered dish or 1 ml of medium in a well of six-well dish), and the medium was replaced with a fresh culture medium the following day. The expression of the target protein was verified by GFP fluorescence.

Confocal imaging

HeLa cells were plated on poly-L-lysine–coated coverslips, and A459/RPE-1 cells were seeded on collagen-coated coverslips. Cells were fixed with warm 4% paraformaldehyde for 10 min at 37°C, permeabilized for 5 min in 0.1% Triton X-100, and blocked for 1 hour in 2% bovine serum albumin in phosphate-buffered saline (PBS) (blocking buffer). Coverslips were incubated in a blocking buffer containing diluted primary antibodies and incubated overnight at 4°C. Cells were washed three times for 10 min with blocking buffer and incubated with corresponding Alexa Fluorophore–conjugated secondary antibodies diluted 1:1000 in blocking buffer for 1 hour at room temperature. Cells were washed three times for 10 min with blocking buffer and once with PBS. Coverslips were mounted on a microscopic slide using fluorescence mounting medium (Dako, catalog no. S3023).

Imaging was performed using a Leica SP8 laser scanning confocal microscope and Zeiss LSM880 with AiryScan. Images of primary cilia are presented as maximum intensity projections. Image analysis was done using ImageJ. All the images were prepared for publication using Adobe Photoshop (adjusted contrast and applied 1-pixel Gaussian blur) and then assembled with Adobe Illustrator.

Live-cell imaging rapamycin-based DENN recruitment

Live-cell imaging was performed using LSM-880 confocal microscope upon addition of 100 nM rapamycin (Sigma-Aldrich). Cells were kept at 37°C in 5% CO_2. Frames were captured every 8 s.

Calculation of degree of colocalization

The degree of colocalization of RFP (DENN or RFP alone in the control) with the GFP-Rab constructs was quantified using Imaris Software at the Analysis Workstation of Advanced BioImaging Facility (McGill). RFP-DENN (mitochondrially localized protein) was masked such that only the mitochondrial area is evaluated. Furthermore, images were thresholded automatically using the Imaris algorithm, and the Pearson correlation coefficient (PCC) was calculated between the two indicated fluorescent signals.

Quantification of recruitment rate of DENN domains or GFP-Rab

We used Imaris software to calculate PCC for each frame over time between mCherry and TagBFP. The degree of colocalization (PCC) represents the recruitment of DENN domain on the mitochondria over time. Similarly, PCC was calculated between mCherry and GFP, which represents the recruitment of Rab35 on the mitochondria over time.

Screening of 60 GFP-Rabs

HeLa cells (9000 cells per 100 ml of culture medium) were seeded in each well of a 96-well plate CellCarrier-96 Ultra Microplates (6055302, PerkinElmer). Cells were cotransfected with 100 ng each of individual GFP-Rabs and DENN(x)-mito or RFP-mito using jetPRIME. At 24 hours post-transfection, cells were fixed with 4% paraformaldehyde, washed three times with PBS, and permeabilized for 5 min in 0.1% Triton X-100 in PBS. Following permeabilization, cells were stained with 4′,6-diamidino-2-phenylindole (DAPI) for 5 min diluted in PBS. Last, cells were washed gently with PBS, and 100 µl of PBS was added to each well.

Each transfected well of the 96-well plate was divided into grids and between 70 and 100 images were acquired by the Opera Phenix HCS microscope using a 63× objective. A qualitative assessments of colocalization of GFP-Rabs and DENN or RFP alone at the mito were performed on all the images by eye estimation. Furthermore, all potential hits were further confirmed by imaging each pair using Leica SP8, which provides much higher resolution.

FRAP imaging

FRAP experiments were carried out on a Zeiss LSM780 laser scanning confocal microscope (Carl Zeiss, Germany). Cells were cultured in 35-mm glass-bottom petri dishes (Lab-Tek II Chamber, USA) and maintained on the microscopy incubator at 5% CO_2 and 37°C. Imaging was performed using a 100×/1.46 numerical aperture Plan-Apochromat oil objective at 5× optical zoom. FRAP conditions were optimized as follows: A region of interest encompassing the centriole was selected (~2.3 µm by 2.3 µm) and photobleached at 100% laser power (488-nm argon laser) with 200 iterations. Prebleach and postbleach time series images were collected at 2-s intervals for 5 to 8 min. Cells were excited by a 488-nm argon laser for GFP-Rab10 or GFP and a 561-nm diode pumped solid state (DPSS) laser with dTomato-Centrin-1, centriolar marker, respectively.

FRAP image analysis

For quantification of the centrosome FRAP experiments, fluorescence intensity was measured using ImageJ software with plugins provided by Stowers Institute. The square measurement region was set to ~2.3 µm by 3 µm. The average intensity of the image was subtracted at each time point as background. Recovery intensities were fit to an exponential curve, described by the following equation: $I(t) = b + I_E (1 - e^{-t/\tau})$, where I is the intensity, I_E is the maximum intensity, t is the time, and τ is an intermediate variable. I_E was identical to the fraction recovered, and τ was used to calculate a recovery half-time ($t_{1/2}$), by the following equation: $t_{1/2} = -\ln 0.5 \times \tau = 0.69\ \tau$. The fluorescence recovery curves were calculated from the averaged values. Statistical analysis of fraction recovered (%) and $t_{1/2}$ was performed in Microsoft Excel (Microsoft Corporation, USA).

Primary cilia induction

A549 or RPE-1 cells were grown in regular culture media until they became fully confluent. Both cell lines were serum-starved for 24 hours. Following starvation, cells were fixed and stained for cilia marker (Ac-tubulin).

SAG treatment

WT or DENND2B KO cells were grown to confluency and cultured in serum-free medium for 24 hours to induce ciliogenesis. Next, serum-free culture medium containing 200 nM Smoothened agonist (SAG) (EMD Milipore, catalog # 566661) was added to cells for 24 hours. Then, cells were washed in PBS, and RNA was extracted as per the method described in the quantitative polymerase chain reaction (PCR) protocol.

Rho activator II (catalog no. CN03) treatment

WT or DENND2B KO cells were grown to confluency and cultured in serum-free medium for 24 hours to induce ciliogenesis. After 24 hours of starvation, serum-free culture medium containing CN03 (1 µg/ml) was added to cells for 6 hours. Then, cells were processed for confocal imaging.

Real-time quantitative PCR

Total RNA was extracted from A549 cells using the RNeasy Mini Kit (QIAGEN), and 500 ng of RNA was used for the cDNA synthesis using the iScript Reverse Transcription Supermix (Bio-Rad Laboratories). Real-time quantitative PCR was performed using the Bio-Rad CFX Connect Real-Time PCR Detection System with SsoFast EvaGreen Supermix (Bio-Rad Laboratories). The values were expressed as fold change in mRNA expression in cells relative to control WT cells (untreated) using TATA-box binding protein and β-2-microglobulin as endogenous controls. The primer sequences (5′ → 3′) used in this study were as follows: Gli1 (forward) GAAGACCTCTCCAGCTTGGA and Gli1 (reverse) GGCTGA-CAGTATAGGCAGAG.

Protein purification

GST-MICAL-L2-C and GST-Rhotekin RBD proteins were expressed in *Escherichia coli* BL21 (500 µM isopropyl β-D-1-thiogalactopyranoside; Wisent Bioproducts; at room temperature for 16 hours) and purified using standard procedure in tris buffer [20 mM tris (pH 7.4), 100 mM NaCl, 10 mM $MgCl_2$, and 1 mM dithiothreitol] supplemented with protease inhibitors.

Biochemical assays
Immunoblot of cell lysate

To analyze levels of p-Rab10, cells were lyzed in phospho-lysis buffer [20 mM Hepes, 100 mM NaCl, 1 mM dithiothreitol, 1% Triton X-100 (pH 7.4), 5 mM sodium pyrophosphate, 500 nM okadaic acid, 1 mM Na_3VO_4, and 10 mM NaF], supplemented with protease inhibitors [0.83 mM benzamidine, 0.20 mM phenylmethylsulfonyl

fluoride, aprotinin (0.5 mg/ml), and leupeptin (0.5 mg/ml)]. Cell lysates were centrifuged at 21,130g for 10 min at 4°C, and the supernatant was resolved by SDS–polyacrylamide gel electrophoresis (PAGE) and processed for Western blotting.

Coimmunoprecipitation
HEK-293T cells grown to 60% confluency in 15-cm dishes were transfected with Flag-tagged or GFP-tagged constructs. At 24 hours post-transfection, cells were gently washed with PBS, scraped into lysis buffer [20 mM Hepes, 100 mM NaCl, 0.5 mM dithiothreitol, 10 mM MgCl$_2$, and 1% Triton X-100 (pH 7.4)] supplemented with protease inhibitors, incubated for 20 min on a rocker at 4°C, and the lysates were centrifuged at 305,000g for 15 min at 4°C. For Flag immunoprecipitation, supernatants were incubated with prewashed protein G beads–Sepharose beads (GE Healthcare) for 1 hour (preclearing step). Following preclearing, supernatants were incubated with protein G–Sepharose beads and the anti-Flag antibody for 2 hours at 4°C. Beads coupled to the Flag antibody were washed three times with the same lysis buffer, eluted in SDS-PAGE sample buffer, resolved by SDS-PAGE, and processed for immunoblotting.

Effector pull-down assay
Cells were gently washed with PBS, lyzed in lysis buffer [20 mM Hepes, 100 mM NaCl, 20 mM MgCl$_2$, and 1% Triton X-100 (pH 7.4)] supplemented with protease inhibitors, and incubated for 20 min on a rocker at 4°C, and the lysates were centrifuged at 305,000g for 15 min at 4°C. For GST pull-down experiments, supernatants were incubated with GST fusion proteins precoupled to glutathione-Sepharose beads for 1 hour at 4°C. GST beads attached to the fusion proteins were washed three times with the same lysis buffer, eluted in SDS-PAGE sample buffer, resolved by SDS-PAGE, and processed for immunoblotting.

Immunoblot
Lysates were run on large 10% polyacrylamide gels and transferred to nitrocellulose membranes. Proteins on the blots were visualized by Ponceau staining. Blots were then blocked with 5% milk in tris-buffered saline with 0.1% Tween 20 (TBST) for 1 hour followed by incubation with antibodies O/N at 4°C diluted in 5% milk in TBST. The next day, blots were washed three times with TBST. Then, the peroxidase-conjugated secondary antibody was incubated in a 1:5000 dilution in TBST with 5% milk for 1 hour at room temperature followed by washes.

Zebrafish
WT TL zebrafish (*Danio rerio*) were bred and maintained according to standard procedures (*70*). All experiments were performed in compliance with the guidelines of the Canadian Council for Animal Care. An antisense MO was designed (Gene Tools) to bind and inhibit specifically the ATG site of the zebrafish *dennd2b* transcript targeting the following sequence (CTGTCAAAGGG AGATGACT-GCCAAC). The standard control MO (CCTCTTACCTCAGTTA CAATTTATA) was used as a control. Injections of 1 nl volumes of an antisense or control MO at a concentration of 0.1 mM were made directly into one-cell stage embryos. For confocal examination, larvae aged 13 hpf were fixed in 4% paraformaldehyde overnight at 4°C. After fixation, the larvae were rinsed several times (1 hour) with PBS, then incubated in freshly prepared block solution containing primary antibody against Ac-tubulin antibody (IF-1:1000) from Cell Signaling Technology (D20G3) overnight at 4°C, washed, and followed by 4 hours of incubation with block solution containing a secondary antibody (1:4000; Alexa Fluor 488 nm, Invitrogen). Labeled zebrafish were washed several times with PBS and mounted on a slide in 70% glycerol before imaging.

Rescue experiment
Human DENND2B mRNAs were transcribed from Not I–linearized pCS2+ using SP6 polymerase with the mMESSAGE Machine Kit (Thermo Fisher Scientific). The mRNA was diluted in nuclease-free water with 0.05% Fast Green (Sigma-Aldrich) to a final concentration of 30 ng/µl and backfilled in a pulled (Sutter Instrument Company) thin-walled bromosilicate capillary tube and pressure-injected into the cell using a PicoSpritzer III (General Valve).

Statistics
Graphs were prepared using GraphPad Prism software. All statistical tests were performed using SPSS. For all data, normality test was performed before determining the appropriate statistical test. For normally distributed data, comparisons were made using either *t* test or one-way analysis of variance (ANOVA) with either Tukey's post hoc multiple comparisons test or Dunnett's test. For nonnormally distributed data, comparisons were made using Mann-Whitney *U* test or Kruskal-Wallis test. All data are shown as the means ± SEM with $P < 0.05$ considered statistically significant.

REFERENCES AND NOTES
1. M. Zerial, H. McBride, Rab proteins as membrane organizers. *Nat. Rev. Mol. Cell Biol.* **2**, 107–117 (2001).
2. Y. Homma, S. Hiragi, M. Fukuda, Rab family of small GTPases: An updated view on their regulation and functions. *FEBS J.* **288**, 36–55 (2021).
3. H. Stenmark, Rab GTPases as coordinators of vesicle traffic. *Nat. Rev. Mol. Cell Biol.* **10**, 513–525 (2009).
4. H. Stenmark, V. M. Olkkonen, The Rab GTPase family. *Genome Biol.* **2**, REVIEWS3007 (2001).
5. A. D. Shapiro, S. R. Pfeffer, Quantitative analysis of the interactions between prenyl Rab9, GDP dissociation inhibitor-α, and guanine nucleotides. *J. Biol. Chem.* **270**, 11085–11090 (1995).
6. Y.-W. Wu, K.-T. Tan, H. Waldmann, R. S. Goody, K. Alexandrov, Interaction analysis of prenylated Rab GTPase with Rab escort protein and GDP dissociation inhibitor explains the need for both regulators. *Proc. Natl. Acad. Sci. U.S.A.* **104**, 12294–12299 (2007).
7. P. Chavrier, J.-P. Gorvel, E. Stelzer, K. Simons, J. Gruenberg, M. Zerial, Hypervariable C-terminal domain of rab proteins acts as a targeting signal. *Nature* **353**, 769–772 (1991).
8. F. Li, L. Yi, L. Zhao, A. Itzen, R. S. Goody, Y.-W. Wu, The role of the hypervariable C-terminal domain in Rab GTPases membrane targeting. *Proc. Natl. Acad. Sci. U.S.A.* **111**, 2572–2577 (2014).
9. A. Barbara Dirac-Svejstrup, T. Sumizawa, S. R. Pfeffer, Identification of a GDI displacement factor that releases endosomal Rab GTPases from Rab-GDI. *EMBO J.* **16**, 465–472 (1997).
10. U. Sivars, D. Aivazian, S. R. Pfeffer, Yip3 catalyses the dissociation of endosomal Rab-GDI complexes. *Nature* **425**, 856–859 (2003).
11. S. Schoebel, L. Katharina Oesterlin, W. Blankenfeldt, R. Sidney Goody, A. Itzen, RabGDI displacement by DrrA from *Legionella* is a consequence of its guanine nucleotide exchange activity. *Mol. Cell* **36**, 1060–1072 (2009).
12. J. Blümer, J. Rey, L. Dehmelt, T. Mazel, Y.-W. Wu, P. Bastiaens, R. S. Goody, RabGEFs are a major determinant for specific Rab membrane targeting. *J. Cell Biol.* **200**, 287–300 (2013).
13. F. A. Barr, Rab GTPases and membrane identity: Causal or inconsequential? *J. Cell Biol.* **202**, 191–199 (2013).
14. J. Cherfils, M. Zeghouf, Regulation of small GTPases by GEFs, GAPs, and GDIs. *Physiol. Rev.* **93**, 269–309 (2013).
15. A. L. Marat, H. Dokainish, P. S. McPherson, DENN domain proteins: Regulators of Rab GTPases. *J. Biol. Chem.* **286**, 13791–13800 (2011).

16. S.-i. Yoshimura, A. Gerondopoulos, A. Linford, D. J. Rigden, F. A. Barr, Family-wide characterization of the DENN domain Rab GDP-GTP exchange factors. *J. Cell Biol.* **191**, 367–381 (2010).

17. A. L. Marat, M. S. Ioannou, P. S. McPherson, Connecdenn 3/DENND1C binds actin linking Rab35 activation to the actin cytoskeleton. *Mol. Biol. Cell* **23**, 163–175 (2012).

18. P. D. Allaire, A. L. Marat, C. Dall'Armi, G. Di Paolo, P. S. McPherson, B. Ritter, The Connecdenn DENN domain: A GEF for Rab35 mediating cargo-specific exit from early endosomes. *Mol. Cell* **37**, 370–382 (2010).

19. M. S. Ioannou, E. S. Bell, M. Girard, M. Chaineau, J. N. R. Hamlin, M. Daubaras, A. Monast, M. Park, L. Hodgson, P. S. McPherson, DENND2B activates Rab13 at the leading edge of migrating cells and promotes metastatic behavior. *J. Cell Biol.* **208**, 629–648 (2015).

20. A. K. Gillingham, R. Sinka, I. L. Torres, K. S. Lilley, S. Munro, Toward a comprehensive map of the effectors of rab GTPases. *Dev. Cell* **31**, 358–373 (2014).

21. O. E. Blacque, N. Scheidel, S. Kuhns, Rab GTPases in cilium formation and function. *Small GTPases* **9**, 76–94 (2018).

22. P. Satir, S. Tvorup Christensen, Overview of structure and function of mammalian cilia. *Annu. Rev. Physiol.* **69**, 377–400 (2007).

23. J. F. Reiter, M. R. Leroux, Genes and molecular pathways underpinning ciliopathies. *Nat. Rev. Mol. Cell Biol.* **18**, 533–547 (2017).

24. M. Mirvis, T. Stearns, W. James Nelson, Cilium structure, assembly, and disassembly regulated by the cytoskeleton. *Biochem. J.* **475**, 2329–2353 (2018).

25. R. Rohatgi, W. J. Snell, The ciliary membrane. *Curr. Opin. Cell Biol.* **22**, 541–546 (2010).

26. A. Knödler, S. Feng, J. Zhang, X. Zhang, A. Das, J. Peränen, W. Guo, Coordination of Rab8 and Rab11 in primary ciliogenesis. *Proc. Natl. Acad. Sci. U.S.A.* **107**, 6346–6351 (2010).

27. I. Göhring, A. Tagariello, S. Endele, C. C. Stolt, M. Ghassibé, M. Fisher, C. T. Thiel, U. Trautmann, A. Vikkula, A. Winterpacht, D. R. FitzPatrick, A. Rauch, Disruption of ST5 is associated with mental retardation and multiple congenital anomalies. *J. Med. Genet.* **47**, 91–98 (2010).

28. S. Pistor, T. Chakraborty, K. Niebuhr, E. Domann, J. Wehland, The ActA protein of Listeria monocytogenes acts as a nucleator inducing reorganization of the actin cytoskeleton. *EMBO J.* **13**, 758–763 (1994).

29. I. Kouranti, M. Sachse, N. Arouche, B. Goud, A. Echard, Rab35 regulates an endocytic recycling pathway essential for the terminal steps of cytokinesis. *Curr. Biol.* **16**, 1719–1725 (2006).

30. D. J. Strick, L. A. Elferink, Rab15 effector protein: A novel protein for receptor recycling from the endocytic recycling compartment. *Mol. Biol. Cell* **16**, 5699–5709 (2005).

31. B. D. Grant, J. G. Donaldson, Pathways and mechanisms of endocytic recycling. *Nat. Rev. Mol. Cell Biol.* **10**, 597–608 (2009).

32. N. A. Zaghloul, S. A. Brugmann, The emerging face of primary cilia. *Genesis* **49**, 231–246 (2011).

33. L. Liu, J.-Q. Sheng, M.-R. Wang, Y. Gan, X.-L. Wu, J.-Z. Liao, D.-A. Tian, X.-X. He, P.-Y. Li, Primary cilia blockage promotes the malignant behaviors of hepatocellular carcinoma via induction of autophagy. *Biomed. Res. Int.* **2019**, 1–14 (2019).

34. M. V. Nachury, A. V. Loktev, Q. Zhang, C. J. Westlake, J. Peränen, A. Merdes, D. C. Slusarski, R. H. Scheller, J. F. Bazan, V. C. Sheffield, P. K. Jackson, A core complex of BBS proteins cooperates with the GTPase Rab8 to promote ciliary membrane biogenesis. *Cell* **129**, 1201–1213 (2007).

35. S. Kuhns, C. Seixas, S. Pestana, B. Tavares, R. Nogueira, R. Jacinto, J. S. Ramalho, J. C. Simpson, J. S. Andersen, A. Echard, S. S. Lopes, D. C. Barral, O. E. Blacque, Rab35 controls cilium length, function and membrane composition. *EMBO Rep.* **20**, e47625 (2019).

36. H. S. Dhekne, I. Yanatori, R. C. Gomez, F. Tonelli, F. Diez, B. Schüle, M. Steger, D. R. Alessi, S. R. Pfeffer, A pathway for parkinson's disease LRRK2 kinase to block primary cilia and sonic hedgehog signaling in the brain. *eLife* **7**, e40202 (2018).

37. R. W. Tucker, A. B. Pardee, K. Fujiwara, Centriole ciliation is related to quiescence and DNA synthesis in 3T3 cells. *Cell* **17**, 527–535 (1979).

38. J. Lee, D. H. Oh, K. C. Park, J. E. Choi, J. B. Kwon, J. Lee, K. Park, H. J. Sul, Increased primary cilia in idiopathic pulmonary fibrosis. *Mol. Cell* **41**, 224–233 (2018).

39. D. K. Breslow, A. J. Holland, Mechanism and regulation of centriole and cilium biogenesis. *Annu. Rev. Biochem.* **88**, 691–724 (2019).

40. S. Graser, Y.-D. Stierhof, S. B. Lavoie, O. S. Gassner, S. Lamla, M. L. Clech, E. A. Nigg, Cep164, a novel centriole appendage protein required for primary cilium formation. *J. Cell Biol.* **179**, 321–330 (2007).

41. B. Delaval, L. Covassin, N. D. Lawson, S. Doxsey, Centrin depletion causes cyst formation and other ciliopathy-related phenotypes in zebrafish. *Cell Cycle* **10**, 3964–3972 (2011).

42. X. Wu, M. J. Bradley, Y. Cai, D. Kümmel, E. M. De La Cruz, F. A. Barr, K. M. Reinisch, Insights regarding guanine nucleotide exchange from the structure of a DENN-domain protein complexed with its Rab GTPase substrate. *Proc. Natl. Acad. Sci. U.S.A.* **108**, 18672–18677 (2011).

43. G. Kulasekaran, M. Chaineau, V. E. C. Piscopo, F. Verginelli, M. Fotouhi, M. Girard, Y. Tang, R. Dali, R. Lo, S. Stifani, P. S. McPherson, An Arf/Rab cascade controls the growth and invasiveness of glioblastoma. *J. Cell Biol.* **220**, e202004229 (2021).

44. Y. Homma, M. Fukuda, Rabin8 regulates neurite outgrowth in both GEF activity-dependent and -independent manners. *Mol. Biol. Cell* **27**, 2107–2118 (2016).

45. H. Sano, G. R. Peck, A. N. Kettenbach, S. A. Gerber, G. E. Lienhard, Insulin-stimulated GLUT4 protein translocation in adipocytes requires the Rab10 guanine nucleotide exchange factor Dennd4C. *J. Biol. Chem.* **286**, 16541–16545 (2011).

46. M. Cabrera, C. Ungermann, Guanine nucleotide exchange factors (GEFs) have a critical but not exclusive role in organelle localization of rab GTPases. *J. Biol. Chem.* **288**, 28704–28712 (2013).

47. S. Yoshida, K. Aoki, K. Fujiwara, T. Nakakura, A. Kawamura, K. Yamada, M. Ono, S. Yogosawa, K. Yoshida, The novel ciliogenesis regulator dyrk2 governs hedgehog signaling during mouse embryogenesis. *eLife* **9**, e57381 (2020).

48. G. B. Carballo, J. R. Honorato, G. P. F. de Lopes, T. C. L. de Sampaio E Spohr, A highlight on Sonic hedgehog pathway. *Cell Commun. Signal.* **16**, 11 (2018).

49. P. Niewiadomski, R. Rohatgi, Measuring expression levels of endogenous gli genes by immunoblotting and real-time pcr. *Methods Mol. Biol.* **1322**, 81–92 (2015).

50. A. J. Streets, P. P. Prosseda, A. C. M. Ong, Polycystin-1 regulates ARHGAP35-dependent centrosomal RhoA activation and ROCK signaling. *JCI Insight* **5**, e135385 (2020).

51. A. Pitaval, Q. Tseng, M. Bornens, M. Théry, Cell shape and contractility regulate ciliogenesis in cell cycle–arrested cells. *J. Cell Biol.* **191**, 303–312 (2010).

52. L. Rangel, M. Bernabé-Rubio, J. Fernández-Barrera, J. Casares-Arias, J. Millán, M. A. Alonso, I. Correas, Caveolin-1α regulates primary cilium length by controlling RhoA GTPase activity. *Sci. Rep.* **9**, 1116 (2019).

53. X.-D. Ren, W. B. Kiosses, M. A. Schwartz, Regulation of the small GTP-binding protein Rho by cell adhesion and the cytoskeleton. *EMBO J.* **18**, 578–585 (1999).

54. A. Spektor, W. Y. Tsang, D. Khoo, B. D. Dynlacht, Cep97 and CP110 suppress a cilia assembly program. *Cell* **130**, 678–690 (2007).

55. D. R. Alessi, E. Sammler, LRRK2 kinase in Parkinson's disease. *Science* **360**, 36–37 (2018).

56. Z. Liu, N. Bryant, R. Kumaran, A. Beilina, A. Abeliovich, M. R. Cookson, A. B. West, LRRK2 phosphorylates membrane-bound Rabs and is activated by GTP-bound Rab7L1 to promote recruitment to the trans-Golgi network. *Hum. Mol. Genet.* **27**, 385–395 (2018).

57. Y. Sobu, P. S. Wawro, H. S. Dhekne, W. M. Yeshaw, S. R. Pfeffer, Pathogenic LRRK2 regulates ciliation probability upstream of tau tubulin kinase 2 via Rab10 and RILPL1 proteins. *Proc. Natl. Acad. Sci. U.S.A.* **118**, e2005894118 (2021).

58. H. Kobayashi, K. Etoh, N. Ohbayashi, M. Fukuda, Rab35 promotes the recruitment of Rab8, Rab13 and Rab36 to recycling endosomes through MICAL-L1 during neurite outgrowth. *Biol. Open* **3**, 803–814 (2014).

59. H. Bagci, N. Sriskandarajah, A. Robert, J. Boulais, I. E. Elkholi, V. Tran, Z.-Y. Lin, M.-P. Thibault, N. Dubé, D. Faubert, D. R. Hipfner, A.-C. Gingras, J.-F. Côté, Mapping the proximity interaction network of the Rho-family GTPases reveals signalling pathways and regulatory mechanisms. *Nat. Cell Biol.* **22**, 120–134 (2020).

60. C. Guilluy, A. D. Dubash, R. García-Mata, Analysis of RhoA and Rho GEF activity in whole cells and the cell nucleus. *Nat. Protoc.* **6**, 2050–2060 (2011).

61. M. S. Sajib, F. T. Zahra, R. G. Akwii, C. M. Mikelis, Identification of Rho GEF and RhoA activation by pull-down assays. *Methods Mol. Biol.* **2193**, 97–109 (2021).

62. E. M. Valente, R. O. Rosti, E. Gibbs, J. G. Gleeson, Primary cilia in neurodevelopmental disorders. *Nat. Rev. Neurol.* **10**, 27–36 (2014).

63. N. Huang, D. Zhang, F. Li, P. Chai, S. Wang, J. Teng, J. Chen, M-Phase Phosphoprotein 9 regulates ciliogenesis by modulating CP110-CEP97 complex localization at the mother centriole. *Nat. Commun.* **9**, 4511 (2018).

64. M. Higgins, I. Obaidi, T. M. Morrow, Primary cilia and their role in cancer. *Oncol. Lett.* **17**, 3041–3047 (2019).

65. M. Steger, F. Tonelli, G. Ito, P. Davies, M. Trost, M. Vetter, S. Wachter, E. Lorentzen, G. Duddy, S. Wilson, M. A. S. Baptista, B. K. Fiske, M. J. Fell, J. A. Morrow, A. D. Reith, D. R. Alessi, M. Mann, Phosphoproteomics reveals that Parkinson's disease kinase LRRK2 regulates a subset of Rab GTPases. *eLife* **5**, e12813 (2016).

66. Z. Liu, E. Xu, H. T. Zhao, T. Cole, A. B. West, LRRK2 and Rab10 coordinate macropinocytosis to mediate immunological responses in phagocytes. *EMBO J.* **39**, e104862 (2020).

67. T. Matsui, T. Itoh, M. Fukuda, Small GTPase Rab12 regulates constitutive degradation of transferrin receptor. *Traffic* **12**, 1432–1443 (2011).

68. T. Tsuboi, M. Fukuda, Rab3A and Rab27A cooperatively regulate the docking step of dense-core vesicle exocytosis in PC12 cells. *J. Cell Sci.* **119**, 2196–2203 (2006).

69. M. Ishida, N. Ohbayashi, Y. Maruta, Y. Ebata, M. Fukuda, Functional involvement of Rab1A in microtubule-dependent anterograde melanosome transport in melanocytes. *J. Cell Sci.* **125**, 5177–5187 (2012).

70. M. Westerfield, *The Zebrafish Book. A Guide for the Laboratory Use of Zebrafish (Danio rerio)* (University of Oregon Press, ed. 3, 1995).